MDPI

Article

Prescribed Performance Adaptive Balance Control for Reaction Wheel-Based Inverted Pendulum-Type Cubli Rovers in Asteroid

He Huang [1,2,*]![ORCID], Zejian Li [1], Zongyi Guo [1,2], Jianguo Guo [1], Le Suo [3] and Haoliang Wang [4]

1   Institute of Precision Guidance and Control, Northwestern Polytechnical University, Xi'an 710072, China
2   Ningbo Institute of Northwestern Polytechnical University, Ningbo 315103, China
3   Institute of Remote Sensing Satellite, China Academy of Space Technology, Beijing 100094, China
4   China Academy of Launch Vehicle Technology, Beijing 100076, China
*   Correspondence: huanghe1984@nwpu.edu.cn

Abstract: This paper investigates the issue of balance control for reaction-wheeled inverted pendulum-type Cubli Rovers on asteroids, and an adaptive control scheme is proposed via the prescribed performance control technique. The main feature lies in the fact that the transient behavior is satisfied which is required critically in the environment of asteroids. The attitude model of reaction-wheeled inverted pendulum-type Cubli Rovers is first constructed by virtue of the momentum moment theorem and Eulerian kinematics. Based on that, the gravitational field in the asteroid is described and the avoiding jumping condition is analyzed. Then, an adaptive prescribed performance control (APPC) method is proposed to obtain the fine tracking performance of the equilibrium error such that the inverted pendulum-type Cubli Rovers achieve the self-balancing motion. The proposed method is capable of ensuring the tracking errors inside the preset boundary functions, and the asymptotic stability of all states in the closed-loop system is guaranteed via the Lyapunov stability theory. The simulation and comparison results on the environment of asteroids verify the effectiveness and superiority of the presented control law.

Keywords: cubli rovers; adaptive prescribed performance control; balancing motion; asteroid; reaction wheel

1. Introduction

Scientific exploration of small-bodies has attracted much attention and interest during recent decades and plays an important role in the exploration of the Solar System. The successful exploration mission of asteroids 433 Eros and 25143 Itokawa, especially the operation of the Hayabusa 2 spacecraft at asteroid 162173 Ryugu, showed the strong feasibility of operating a spacecraft in close proximity to small-bodies. The causes of these explorations are based on several reasons, such as the exploration of early formation stages of the solar system and planetary defense.

The gravity of an asteroid is very weak, and the irregular gravitational field around an asteroid also perturbs the state of a spacecraft [1]. Thus, the traditional roller rover cannot move on the surface of small objects for inspection and detection. Reaction wheel-based pendulum-type Cubli Rovers are suitable as asteroid surface rovers, which can generate jumping behavior by their flywheels or perform a tumbling motion. The use of ballistic jump landing and the tumbling of the detector attitude to achieve the movement of the surface of the asteroid has gathered increased interest. The main advantage lies in the long-range and large-area detection on the surface of small-bodies can be achieved by jumping. Meanwhile, the attitude and position of the rover can be moved by internal angular momentum exchange, which is mechanically simple and easy to implement without chemical propulsion and is not affected by a dusty environment. There are two kinds of ideas for the tumbling and jumping patrol in literature. One is to drive an external mechanical structure to contact the surface of the star to generate a rebound force [2]. On

the other hand, the collision between the spacecraft and the surface of the small celestial body produces a rebound force [3]. In [4–6], the satellite on-orbit attitude control process around small celestial bodies and the gravity field of small celestial bodies are investigated. The Philae lander of the ESA Rosetta mission and the MINERVA-II and MASCOT small ballistic jump landers of the Japanese Hayabusa 2 mission have successfully conducted small-body jump landing tests [7,8]. However, the Cubli Rovers are suitable as jump probes on the surface of asteroids and no relevant studies have been found in the open literature.

In the current literature, there have been investigations on Cubli [9]. The Cubli is similar to the 3-D inverted pendulum system, and a 3-D inverted pendulum system [10] was gradually evolved. Different from the linear trolley control in the traditional inverted pendulum, the 3-D inverted pendulum often used a three-axis flywheel and housing to form a momentum exchange system. It was originally developed by ETH Zurich as a 15 cm × 15 cm × 15 cm robot that can stably stand upside down with one vertex of a cube and can jump and roll. In terms of control, in [9], the vertical position control of the Cubli one-dimensional prototype was first performed using the LQR method. In [11], the dynamics of 3-D systems were modeled based on Kane's equations, and a system identification method was provided, using LQR for stable control of the linearized model. Ref. [12] proposed an optimal-size cube robot based on parameter optimization, and through feedforward control, it achieved self-balancing stability. A feedback controller was proposed based on the backstepping method for balance control [13], and the feedback linearization was used to design the controller to track the take-off trajectory segment. Ref. [14] used the Lagrangian method and Kane method to establish an attitude control model and verified the validity of the model through simulation. To maintain the balance on the Cubli frame, an LQR controller based on a Lagrangian derivation of the dynamics was designed, which utilized the state variables of the frame angle and its angular acceleration, as well as the wheel angle and its angular acceleration [15]. A method for feedback control using quaternions to describe attitude is proposed in the literature [16]. An adaptive robust control is presented to balance the uncertain Cubli system on its corner in the literature [17]. However, in the existing kinds of literature, the special environment of the asteroid surface and the angular velocity limitation have not been considered, and the dynamic performance requirement has been not considered yet.

A so-called prescribed performance control (PPC) method to ensure the prescribed performance output has been proposed in [18]. Two robust adaptive control schemes for single-input single-output (SISO) strict feedback nonlinear systems possessing unknown nonlinearities, capable of guaranteeing prescribed performance bounds are presented in this paper [19]. In [20], a universal, approximation-free state feedback control scheme is designed for unknown pure feedback systems, capable of guaranteeing, for any initial system condition, output tracking with prescribed performance and bounded closed-loop signals. This paper [21] investigates the issue of control design for a class of nonlinear systems with guaranteed prescribed performance. In [22], the authors present a performance-guaranteed adaptive asymptotic tracking control scheme for a class of nonlinear systems with an unknown sign-switching control direction. The study [23] develops a novel robust distributed estimation algorithm, capable of achieving practically zero average tracking error even for fast time-varying reference signals. The PPC method is beginning to attract the attention of researchers in various fields and it is also widely used especially in the aerospace field. The PPC has been applied in satellite attitude control [24] and flight vehicles [25]. In [26], based on the novel performance function and error transformation constraints, the attitude tracking error is converted into a new error system that guarantees the desired transient and steady-state responses for the tracking error. In this paper [27], a nonlinear disturbance-observer-based fault-tolerant attitude control scheme is developed for the combined spacecraft with prescribed performance. Performance in the light of convergence time, stability and accuracy with inertia uncertainty, actuator saturation and external disturbance can be prescribed.

The PPC approach, as a control methodology to conduct the dynamic or transient performance of the system, provides a new idea for the control system design of Cubli Rovers. Thus, inspired by the PPC method, the paper presents an adaptive PPC for reaction wheel-based Cubli Rovers to ensure the success of the balance control, and meanwhile, the avoiding jumping condition is also considered. The main features of this paper are twofold:

(1) An adaptive prescribed performance control scheme is proposed for the attitude system of reaction wheel-based inverted pendulum-type Cubli Rovers in the environment of the asteroid to achieve fine transient performance in the balancing motion. Asymptotic stability of the tracking errors is guaranteed even under uncertainties.

(2) Based on the knowledge of attitude dynamics, the avoiding jumping condition in the specific gravitational field in the asteroid is analyzed and the proposed control is guaranteed not to leave the ground via the small angular velocity.

The rest of this paper is organized as follows. Section 2 formulates the attitude model for the balancing control for Cubli Rovers and the gravitational field and avoiding jumping condition are analyzed in detail in Section 3. The main theoretical results about the adaptive prescribed performance control are given in Section 4. Section 5 provides simulation results and Section 6 concludes the paper.

2. Problem Formulation

2.1. Attitude Model of Reaction Wheel-Based Inverted Pendulum-Type Cubli Rovers

The stable stationing of Cubli Rovers on the surface of an asteroid can be formulated as a single-point self-balancing problem. In this part, the attitude model of reaction wheel-based pendulum-type Cubli Rovers is presented for the balancing control. The three momentum wheels of Cubli Rovers are equipped orthogonally on adjacent edges, and the center of mass of the momentum wheels is located at the geometric center of the cube face, as shown in Figure 1.
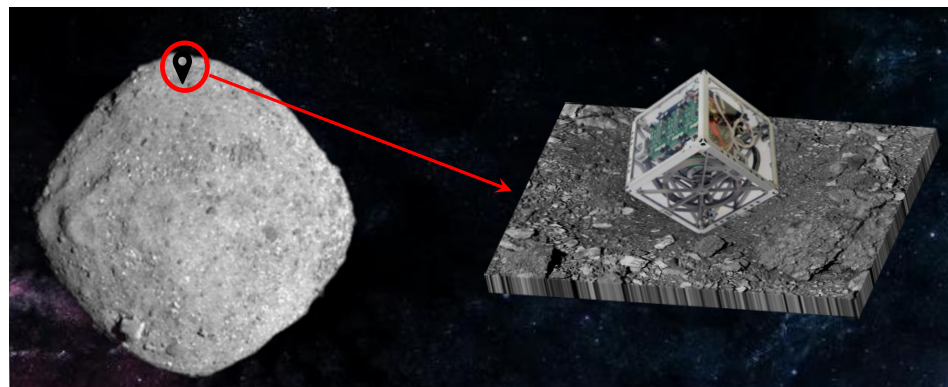
Figure 1. Schematic diagram of reaction wheel-based Cubli Rovers in the asteroid.

Without loss of generality, the model can be appropriately simplified, and it is considered to increase the load on the surface without the momentum wheel to ensure that the cube center of mass coincides with the geometric center, and it can be considered as a symmetrical geometry. Considering the three-degree-of-freedom problem of fixed-point rotation of a rigid body, it is possible to establish the body fixed frame o-xyz with the origin located at the center of mass and the three coordinate axes passing through the center of the geometric surface, respectively.

The coordinate system is established as shown in Figure 2 and the body-fixed frame is used as the inertial frame O-XYZ by selecting the equilibrium position. The Cardan transformation sequence 1-2-3 is used for the transformation between the body-fixed frame to the inertial frame, and the pitch, yaw and roll angles ϕ, θ, ψ are obtained as the attitude angles to describe the attitude of Cubli Rovers. The transformation matrix from the inertial frame to the fixed body frame can be expressed as follows

$$A = \begin{bmatrix} \cos\theta\cos\psi & \sin\phi\sin\theta\cos\psi + \cos\phi\sin\psi & -\cos\phi\cos\psi\sin\theta + \sin\phi\sin\psi \\ -\cos\theta\sin\psi & -\sin\phi\sin\theta\sin\psi + \cos\phi\cos\psi & \cos\phi\sin\theta\sin\psi + \sin\phi\cos\psi \\ \sin\theta & -\sin\phi\cos\theta & \cos\phi\cos\theta \end{bmatrix} \quad (1)$$
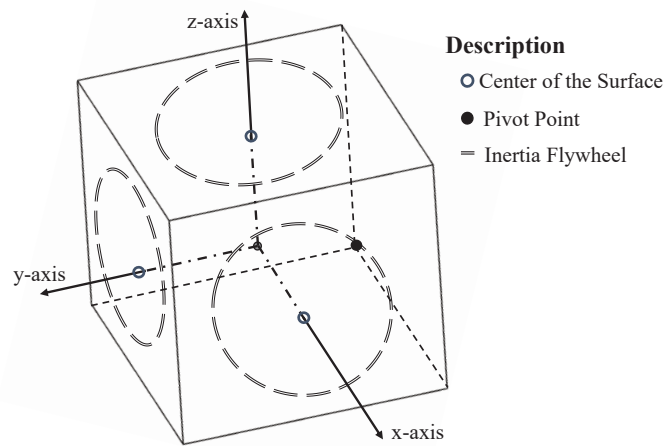

Figure 2. Principle axes of reaction wheel-based Cubli Rovers.

Furthermore, the dynamics of the attitude angles can be represented by the angular velocity which is shown as follows

$$\begin{bmatrix} \dot{\phi} \\ \dot{\theta} \\ \dot{\psi} \end{bmatrix} = \begin{bmatrix} \cos\psi/\cos\theta & -\sin\psi/\cos\theta & 0 \\ \sin\psi & \cos\psi & 0 \\ -\cos\psi\tan\theta & \sin\psi\tan\theta & 1 \end{bmatrix} \begin{bmatrix} \omega_x \\ \omega_y \\ \omega_z \end{bmatrix} \quad (2)$$

According to the Lagrangian mechanics method [13] and the moment of momentum theorem, one has that

$$\dot{P} = M_g + M_T + M_d \quad (3)$$

where $\dot{P}$ is the total momentum of the system without the flywheel momentum, M_g represents the moment generated by gravity on the rotation point of the system, and M_T represents the moment generated by the flywheel. The term M_d represents the resultant torque generated by external disturbances. Note that the possible relative sliding of the ground pivot point is ignored in this paper. According to the moment of momentum theorem, the rate of change of the momentum of the system is equal to the torque produced by the external force acting on the system

$$M_g = r \times mg = \begin{bmatrix} -\frac{l}{2} \\ -\frac{l}{2} \\ -\frac{l}{2} \end{bmatrix} \times A \begin{bmatrix} -\frac{\sqrt{3}}{3}mg^I \\ -\frac{\sqrt{3}}{3}mg^I \\ -\frac{\sqrt{3}}{3}mg^I \end{bmatrix} \quad (4)$$

where r represents the vector radius from the position of the center of mass to the pivot point, m represents the total mass of the Cubli Rovers, l represents the side length, and g^I represents the gravity vector at the current position.

Define $\dot{\omega}$ as the rate of change of the triaxial angular velocity of the shell, and then one has that $\dot{P} = I_0\dot{\omega}$, where I_0 denotes the moment of inertia of the shell. Since the axial direction is defined as the geometric center passing through the side, the inertia products of the inertia tensor matrix I_{xy}, I_{xz}, I_{yz} are ideally set as zero. Therefore, the system model of the attitude rate can be expressed as:

$$\begin{bmatrix} \dot{\omega}_x \\ \dot{\omega}_y \\ \dot{\omega}_z \end{bmatrix} = I_0^{-1} \cdot \dot{P} = I_0^{-1} \cdot M_g + I_0^{-1} \cdot M_T + d \tag{5}$$

where $d = I_0^{-1} \cdot M_d$ represents the disturbances. The flywheel torque M_T is used as the input of the system, which has the dynamic characteristics of the flywheel, that is, the limit and the saturation of the flywheel speed. Finally, the attitude model of reaction wheel-based inverted pendulum-type Cubli Rovers is obtained by (2) and (5).

2.2. Balance Control Issue in Asteroid

Based on the above modeling procedure, the model of traction wheel-based inverted pendulum-type Cubli Rovers is expressed as a multi-variable nonlinear second-order system with disturbances. The task of the balance control is to ensure the stability of the Cubli Rovers when they are set up. It is important for the mission of the rover on the asteroid. However, the balancing control investigated in this paper is different from that on Earth due to the following reasons:

(1) For the Cubli Rovers, the main concern is whether the attitude angle and angular velocity achieve satisfactory dynamic performance. The introduction of a flywheel as the actuator will cause some problems with speed saturation and instantaneous impulse limitation. In addition, due to the three-axes coupling, it is necessary to ensure that the overshoot of the angular velocity of each axis cannot be large to avoid affecting the effective control of other axes, which puts forward performance requirements for the control method.

(2) Due to the existence of a special gravitational field on asteroids, the effect of gravity plays an important role in the balancing control for Cubli Rovers. Unlike the common gravitational field on Earth, the non-uniform gravitational field affects the system balance if the attitude inclination cannot meet the small steady-state error, so the performance requirement of steady-state error is proposed. On the other hand, in the asteroid environment, the centripetal force provided by gravity is limited, so the angular velocity magnitude should be limited at all times during the rotation to avoid the Cubli Rovers from leaving the ground.

Consequently, the dynamic or transient performance of the balancing control for Cubli Rovers, including the overshoot, steady-state error and setting time, is the main focus that determines the mission on the asteroid. Dynamic performance requirements depend on a pre-designed time-varying function with the ability to assign performance limits throughout the procedure. Therefore, time-varying constrained performance functions are applicable for the control design and thus can ensure that multiple performance requirements are met. To sum up, the control goal of the paper is to steer the attitude angles tracking the desired references with the tracking errors always into the preassigned performance functions.

3. Asteroid Environment and Avoiding Jumping Conditions

### 3.1. Basic Description of Gravitational Field in Asteroid

Small-bodies such as asteroids and comets can be patrolled and probed to obtain more information about material properties and topography and becomes a hot point in the field of deep-space exploration. How to ensure that the small spacecraft can move reliably on the surface of small objects is challenging for the current control community. Since the gravitational field of small-bodies is very weak and irregular, the traditional roller rover cannot be used for surface-moving inspection of asteroids. It is one of the important ways of surface movement of small-bodies to adjust the position of the inspector by flywheel control moment and make it roll or jump.

In this paper, let us take the Bennu asteroid as the research object, and the gravitational constant $G = 6.67 \times 10^{-11}$. The density of Bennu obtained by on-orbit optical measurement analysis $\rho = 2670 \text{ kg}/\text{m}^3$ [28], plus the Bennu in the NASA planetary database, and finally, the distribution of the surface gravity value of the asteroid Bennu after triangulation can

be calculated. The gravitational value indicates the magnitude of gravity per unit mass of the object on the asteroid. The gravitational value of asteroid Bennu is the largest at the two poles, located within $2 \sim 2.6 \times 10^{-3}$ N [29]. Meanwhile, the closer to the equator, the smaller the gravity value. This is because the shape of the Bennu asteroid is generally oblate spheroid, the two-stage distance from the center of mass is smaller than that from the equator, and the axis of rotation is generally located at the line connecting the two poles, which makes the gravitational acceleration on the surface of Bennu vary with different latitude. The gravitational field on the surface of the asteroid is quite weak according to the size of the asteroid's volume. The gravitational acceleration is in the range of $10^{-4} \sim 10^{-3}$ m/ s^2.

3.2. Avoiding Jumping Conditions

The motion of the Cubli Rovers is divided into two cases in the 2-D plane, one is stable rotation around a fixed point, and the other is jumping off the ground. In this paper, we consider the single-point self-balancing motion of Cubli Rovers. Therefore, the condition of stable rotation around the fixed point is proposed first. Because the asteroids are not ideal spheres but non-regular, the gravity of the Cubli Rovers in contact with the ground is not perpendicular to the ground but at an angle to the ground normal. Force analysis is shown in Figure 3.
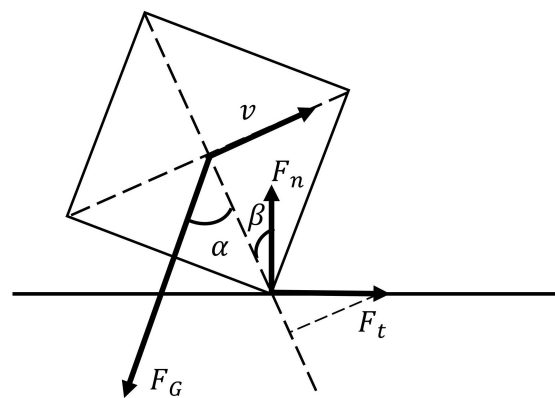
Figure 3. Force analysis for avoiding jumping away from the asteroid.

The Hayabusa 2 team summarized a few real images from the mission to introduce the asteroid surface [30]. The surface environment of the asteroid is relatively complex. In [31,32], the researchers established a detailed surface environment of asteroid rocks and detailed the dynamical relationships during the landing of the probe. In [33], the authors describe the problem of predicting the reachable domain of the hopping rover with full consideration of the asteroid rock surface as well as the gravitational environment, illustrating the influence of topographic conditions on the probe takeoff. As a result, a conclusion can be drawn that Bennu surfaces are covered with boulders and rocks, which made the sample mission decay. However, for the highest shape model 2019 from NASA, the mean length of the triangular meshes is approximately 3.2 m. The self-equilibrium verification is assumed to be a single-point position motion. This also means that Cubli Rovers will not have a large lateral displacement in the control process. When we numerically put the Cubli Rovers [15 cm × 15 cm × 15 cm] on the facets, it can be assumed as a flat surface contact and gravity will not change in such a preliminary study.

The Cubli Rovers mechanically change very little in the vertical direction during the self-balancing motion control, and the degree of influence on the surface is so weak that the deformation of the surface can be neglected. Therefore, the nature of the asteroid surface is simplified in this study, and the landing area of the Cubli Rovers is assumed to be a rigid surface. For more geological types, readers may be referred to [34,35].

From the projection of the external force in the direction perpendicular to the velocity, the centripetal force expression can be derived by

$$F = F_G \cos(\alpha) + F_t \sin(\beta) - F_n \cos(\beta) \tag{6}$$

where $F_G = mg$ denotes the gravitational force, F_t denotes the tangential force generated by the tendency of the shell to move backward at the point of contact with the ground, and F_n denotes the upward support force of the ground on the shell. The centripetal force required during the rotation of the shell around the fixed point.

$$F_r = \frac{\sqrt{2}m\,\omega^2\,l}{2} \tag{7}$$

Therefore, to ensure the stable rotation of the shell does not leave the ground, the condition $F_r \leq F$ should be satisfied, otherwise, the external force will not provide sufficient force, resulting in centrifugal movement of the shell. In the critical state of leaving the surface of the asteroid, the support force F_n tends to zero and the tangential force $F_t = \mu\,F_n$ also tends to zero, so that the condition of the rotational speed is satisfied and reaches the maximum, which can be reduced to the case where only the gravity constrains the system. The relation can be obtained as follows

$$\frac{\sqrt{2}m\,\omega^2\,l}{2} \leq mg\cos(\alpha) \tag{8}$$

Then it follows that

$$\omega \leq \sqrt{\frac{\sqrt{2}g\cos(\alpha)}{l}} \tag{9}$$

Extending to the 3-D case, the projection of gravity is orthogonal to the sagittal path of the center of mass and the fixed point, and the angular velocities of the three axes are orthogonal to each other to find the contrast centripetal force. Then, it can be compared with the projection of gravity on the surface to determine whether the system satisfies the condition of not leaving the ground and can reside stably on the asteroid's surface.

4. Balance Control Based on Adaptive Prescribed Performance Control
4.1. APPC Design

At the expected target position, the inertial frame and the body fixed frame should coincide, that is, the attitude angles ϕ, θ, ψ are zero. Then, the values of tracking target signals are set as $\phi_{ref} = 0$, $\theta_{ref} = 0$, $\psi_{ref} = 0$. Then, the tracking errors of the attitude angles are represented as

$$\begin{aligned} e_\phi &= \phi - \phi_{ref} \\ e_\theta &= \theta - \theta_{ref} \\ e_\psi &= \psi - \psi_{ref} \end{aligned} \tag{10}$$

For the attitude angle system, the angular velocity can be viewed as the input and a virtual input Γ_a for the attitude angle is obtained by

$$\Gamma_a = \begin{bmatrix} \delta_1 & \delta_2 & \delta_3 \end{bmatrix}^T \tag{11}$$

Define the angular rate tracking virtual input state errors as follows

$$\begin{aligned} e_{\omega x} &= \omega_x - \delta_1 \\ e_{\omega y} &= \omega_y - \delta_2 \\ e_{\omega z} &= \omega_z - \delta_3 \end{aligned} \tag{12}$$

Taking the derivatives of the tracking errors yields that

$$
\begin{bmatrix} \dot{e}_\phi \\ \dot{e}_\theta \\ \dot{e}_\psi \end{bmatrix} = \begin{bmatrix} \dot{\phi} - \dot{\phi}_{ref} \\ \dot{\theta} - \dot{\theta}_{ref} \\ \dot{\psi} - \dot{\psi}_{ref} \end{bmatrix} = \begin{bmatrix} \cos\psi/\cos\theta & -\sin\psi/\cos\theta & 0 \\ \sin\psi & \cos\psi & 0 \\ -\cos\psi\tan\theta & \sin\psi\tan\theta & 1 \end{bmatrix} \begin{bmatrix} \omega_x \\ \omega_y \\ \omega_z \end{bmatrix} = G_a \begin{bmatrix} \omega_x \\ \omega_y \\ \omega_z \end{bmatrix} \tag{13}
$$

$$
\begin{bmatrix} \dot{e}_{\omega x} \\ \dot{e}_{\omega y} \\ \dot{e}_{\omega z} \end{bmatrix} = \begin{bmatrix} \dot{\omega}_x \\ \dot{\omega}_y \\ \dot{\omega}_z \end{bmatrix} - \begin{bmatrix} \dot{\delta}_1 \\ \dot{\delta}_2 \\ \dot{\delta}_3 \end{bmatrix} + \begin{bmatrix} d_x \\ d_y \\ d_z \end{bmatrix} \tag{14}
$$

Design the following virtual control law for the subsystems (13)

$$
\begin{aligned}
\Gamma_a &= -G_a^{-1}\lambda_a\varepsilon_a - G_a^{-1}\operatorname{sgn}(\varepsilon_a)k_a\hat{v}_a \\
\dot{\hat{v}}_a &= \eta_a|\varepsilon_a|
\end{aligned} \tag{15}
$$

where $\lambda_a = diag(\lambda_{a1}, \lambda_{a2}, \lambda_{a3})$, $\lambda_{ai} > 0$, $i = 1,2,3$, $\varepsilon_a = \begin{bmatrix} \varepsilon_{a1}, \varepsilon_{a2}, \varepsilon_{a3} \end{bmatrix}^T$, $\operatorname{sgn}(\varepsilon_a) = diag(\operatorname{sgn}(\varepsilon_{a1}), \operatorname{sgn}(\varepsilon_{a2}), \operatorname{sgn}(\varepsilon_{a3}))$, $k_a = diag(k_{a1}, k_{a2}, k_{a3})$, $k_{ai} > 0$, $\hat{v}_a = [\hat{v}_{a1}, \hat{v}_{a2}, \hat{v}_{a3}]^T$, $\eta_a = diag(\eta_{a1}, \eta_{a2}, \eta_{a3})$, $\eta_{ai} > 0$, $i = 1,2,3$, where $\varepsilon_{ai} = \frac{\xi_{ai}}{1-\xi_{ai}^2}$, $\xi_{ai} = \frac{e_{ai}}{\rho_{ai}}(i = 1,2,3)$. ξ_{ai} represents the ratio of the state error to the performance function. When $|\xi_{ai}| < 1$, we can deduce that $-\rho_{ai} < e_{ai} < \rho_{ai}$. They need to be converted to unconstrained variables by using non-linear transformation relations $\varepsilon_{ai} = \frac{\xi_{ai}}{1-\xi_{ai}^2}$. The performance functions are chosen as $\rho_{ai} = (\rho_{ai0} - \rho_{ai\infty})e^{l_{ai}t} + \rho_{ai\infty}(i = 1,2,3)$, where the constants $\rho_{ai0} > \rho_{ai\infty} > 0, l_{ai} < 0$.

For the angular rate subsystem (14), the actual control law can be designed as

$$
\begin{aligned}
u_v &= -I_0\lambda_u\varepsilon_u - I_0\operatorname{sgn}(\varepsilon_u)k_u\hat{v}_u \\
\dot{\hat{v}}_u &= \eta_u|\varepsilon_u|
\end{aligned} \tag{16}
$$

where $\lambda_u = diag(\lambda_{u1}, \lambda_{u2}, \lambda_{u3})$, $\lambda_{ui} > 0$, $i = 1,2,3$, $\varepsilon_u = [\varepsilon_{u1}, \varepsilon_{u2}, \varepsilon_{u3}]^T$, $\operatorname{sgn}(\varepsilon_u) = diag(\operatorname{sgn}(\varepsilon_{u1}), \operatorname{sgn}(\varepsilon_{u2}), \operatorname{sgn}(\varepsilon_{u3}))$, $k_u = diag(k_{u1}, k_{u2}, k_{u3})$, $k_{ui} > 0$, $\hat{v}_u = [\hat{v}_{u1}, \hat{v}_{u2}, \hat{v}_{u3}]^T$, $\eta_u = diag(\eta_{u1}, \eta_{u2}, \eta_{u3})$, $\eta_{ui} > 0$, $i = 1,2,3$, where $\varepsilon_{ui} = \frac{\xi_{ui}}{1-\xi_{ui}^2}$, $\xi_{ui} = \frac{e_{ui}}{\rho_{ui}}(i = 1,2,3)$. ξ_{ai} represents the ratio of the state error to the performance function. When $|\xi_{ui}| < 1$, we can deduce that $-\rho_{ui} < e_{ui} < \rho_{ui}$. They need to be converted to unconstrained variables by using non-linear transformation relations $\varepsilon_{ui} = \frac{\xi_{ui}}{1-\xi_{ui}^2}$. Similarly, the performance boundary functions are set as $\rho_{ui} = (\rho_{ui0} - \rho_{ui\infty})e^{l_{ui}} + \rho_{ui\infty t}(i = 1,2,3)$ where the constants $\rho_{ui0} > \rho_{ui\infty} > 0, l_{ui} < 0$.

Schematic diagram of the proposed control method is shown in Figure 4.
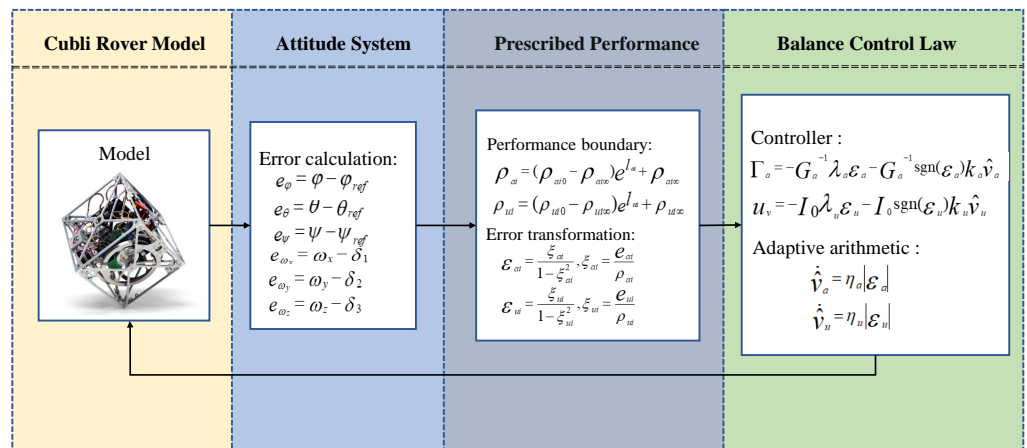

Figure 4. Schematic diagram of the proposed control method.

Remark 1. *The singular point of the matrix G_a is located at $\theta = \frac{\pi}{2} + n\pi$. Considering the actual situation of Cubli Rovers, even when the body is stationary on the ground, $0 < \theta < \frac{\pi}{2}$ will not reach the singular point. Therefore, the matrix G_a is always invertible.*

4.2. Stability Analysis

This part provides the stability analysis of the proposed APPC law. The necessary theorem is given and explained as follows:

Theorem 1 ([36]). *Let $X = \{x \in \Re^n : |x_i| < \Omega_i, i = 1, 2, \ldots, n\}$ be an open set with positive constants Ω_i. Consider the switched system:*

$$\dot{x} = y_q(t, x), x(0) \in X \tag{17}$$

where $y_i : \Re_+ \times x \to \Re^n$ is piecewise continuous and uniformly bounded in t and locally Lipschitz on x; q is the switching signal, which takes its values in a finite set $\{1, \ldots, m\}$ and $m > 1$ is the number of subsystems. Suppose that the state of the system Equations (13) and (14) does not jump at the switching instants. Then there exists a unique and maximal solution $x(t) \in X$ on the time interval $[0, T)$ where $T \leq +\infty$.

Theorem 1 shows that the state must remain in a domain if the initial value lies within a finite time interval. the assumption in Lemma 1 about no jumps at the moment of switching is to ensure the continuity of the state, which is necessary and quite important to guarantee that the constrained performance function is not violated. Note that the switching action takes place in the controller, as shown in the formulation of the control law. In other words, the switching occurs on the right-hand side of the dynamic equation, and therefore, does not cause a jumping action of the state. Therefore, the assumption is reasonable in this paper. This theorem is important for performance-guaranteed control design. Of course, we hope that T can be set as $+\infty$, but it may be not satisfied for any case. In this paper, the proposed control law can ensure $T = +\infty$, which is proven by Theorem 1. Therefore, the basic thought of the proof is described as follows. Firstly the existence and uniqueness of a maximal solution $\sigma(t)$ for a time interval $[0, T)$ is ensured. Then, in the following theorem, we prove that the proposed control scheme guarantees, for $t \in [0, T)$: (i) the boundedness of all signals in the closed-loop system; (ii) seek a contradiction to lead to $T = +\infty$. Finally, we prove that the proposed adaptive control law is analyzed in the following theorem.

Theorem 2. *Consider the system model Equations (13) and (14) and the proposed adaptive prescribed performance control Equations (15) and (16). Assuming that Assumptions 1 and 2 hold, the following statements are satisfied:*

(1)   All signals of the closed-loop system are globally bounded;
(2)   The relations $|e_{ai}| < \rho_{ai}, |e_{ui}| < \rho_{ui}, i = (1, 2, 3)$ are satisfied;
(3)   The error converges to zero asymptotically, that is $e_{ai} \to 0, e_{ui} \to 0, i = (1, 2, 3)$ as $t \to \infty$.

Proof of Theorem 2. Invoking the novel adaptive prescribed performance control (15) and (16), into the system (13) and (14) yields the closed-loop system as follows:

$$\dot{\kappa} = Y(t, \kappa) \tag{18}$$

where $\kappa = [\kappa_{a1}, \kappa_{a2}, \kappa_{a3}, \kappa_{u1}, \kappa_{u2}, \kappa_{u3}]^T$ and the function $Y = [Y_{a1}, Y_{a2}, Y_{a3}, Y_{u1}, Y_{u2}, Y_{u3}]^T$ is represented as

$$
\begin{aligned}
Y_{a1} &= \tfrac{1}{\rho_{a1}}\left[b_1\,G_a\,\Gamma_a - \dot{\rho}_{a1}\,\xi_{a1} - \dot{\phi}_{ref}\right] \\
Y_{a2} &= \tfrac{1}{\rho_{a2}}\left[b_2\,G_a\,\Gamma_a - \dot{\rho}_{a2}\,\xi_{a2} - \dot{\theta}_{ref}\right] \\
Y_{a3} &= \tfrac{1}{\rho_{a3}}\left[b_3\,G_a\,\Gamma_a - \dot{\rho}_{a3}\,\xi_{a3} - \dot{\psi}_{ref}\right] \\
Y_{u1} &= \tfrac{1}{\rho_{u1}}\left[b_1\,I_0^{-1}\,M_g + b_1\,I_0^{-1}\,u_v - \dot{\rho}_{u1}\,\xi_{u1} - \dot{\delta}_1 + d_x\right] \\
Y_{u2} &= \tfrac{1}{\rho_{u2}}\left[b_2\,I_0^{-1}\,M_g + b_2\,I_0^{-1}\,u_v - \dot{\rho}_{u2}\,\xi_{u2} - \dot{\delta}_2 + d_y\right] \\
Y_{u3} &= \tfrac{1}{\rho_{u3}}\left[b_3\,I_0^{-1}\,M_g + b_3\,I_0^{-1}\,u_v - \dot{\rho}_{u3}\,\xi_{u3} - \dot{\delta}_3 + d_z\right]
\end{aligned}
\tag{19}
$$

Note that the trajectory of the system (19) is continuous at the switching instants, and thus, the existence and uniqueness of a maximal solution κ is guaranteed on the time interval $[0, T)$ according to Theorem 1.

Select the Lyapunov function as:

$$
V_{a1} = \frac{1}{2}\ln\left(\frac{1}{1-\xi_{a1}^2}\right) + \frac{k_{a1}\,a_{a1}}{2\,\eta_{a1}}\,\tilde{v}_{a1}^2
\tag{20}
$$

where $\tilde{v}_{a1} = v_{a1} - \hat{v}_{a1}$, a_{a1} is an unknown constant. Taking the derivative of V_{a1} yields that

$$
\begin{aligned}
\dot{V}_{a1} &= \frac{1}{2}\left(1-\xi_{a1}{}^2\right)\left(\left(1-\xi_{a1}^2\right)^{-1}\right)' + \frac{k_{a1}\,a_{a1}}{\eta_{a1}}\,\tilde{v}_{a1}\,\dot{\hat{v}}_{a1} \\
&= \frac{1}{2}\left(1-\xi_{a1}{}^2\right)\left(-\frac{1}{1-\xi_{a1}^2}\right)^2(-2\,\xi_{a1})\,\dot{\xi}_{a1} + \frac{k_{a1}\,a_{a1}}{\eta_{a1}}\,\tilde{v}_{a1}\left(\dot{v}_{a1} - \dot{\hat{v}}_{a1}\right) \\
&= \frac{\xi_{a1}}{1-\xi_{a1}^2}\,\dot{\xi}_{a1} - \frac{k_{a1}\,a_{a1}}{\eta_{a1}}\,\tilde{v}_{a1}\,\dot{\hat{v}}_{a1} \\
&= \varepsilon_{a1}\left(\frac{\dot{e}_\phi}{\rho_{a1}} - \frac{\dot{\rho}_{a1}}{\rho_{a1}{}^2}\,e_\phi\right) - \frac{k_{a1}\,a_{a1}}{\eta_{a1}}\,\tilde{v}_{a1}\,\dot{\hat{v}}_{a1} \\
&= \frac{\varepsilon_{a1}}{\rho_{a1}}\left(\dot{e}_\phi - \frac{\dot{\rho}_{a1}}{\rho_{a1}}\,e_\phi\right) - \frac{k_{a1}\,a_{a1}}{\eta_{a1}}\,\tilde{v}_{a1}\,\dot{\hat{v}}_{a1}
\end{aligned}
\tag{21}
$$

for the e_ϕ component in the vector, define an extraction vector: $b_1 = \begin{bmatrix} 1 & 0 & 0 \end{bmatrix}$, used to extract the quantity of e_ϕ active channels in the system model. According to the expression of (13) and (15) one has that

$$
\begin{aligned}
\dot{V}_{a1} &= \frac{\varepsilon_{a1}}{\rho_{a1}}\left(b_{a1}(G_a\,\Gamma_a) - \frac{\dot{\rho}_{a1}}{\rho_{a1}}\,e_\phi\right) - \frac{k_{a1}\,a_{a1}}{\eta_{a1}}\,\tilde{v}_{a1}\,\dot{\hat{v}}_{a1} \\
&= \frac{\varepsilon_{a1}}{\rho_{a1}}\left(-\lambda_{a1}\,\varepsilon_{a1} - \mathrm{sgn}(\varepsilon_{a1})\,k_{a1}\,\hat{v}_{a1} - \frac{\dot{\rho}_{a1}}{\rho_{a1}}\,e_\phi\right) - \frac{k_{a1}\,a_{a1}}{\eta_{a1}}\,\tilde{v}_{a1}\,\dot{\hat{v}}_{a1} \\
&\leq -\frac{\lambda_{a1}}{\rho_{a1}}\,\varepsilon_{a1}^2 - \frac{k_{a1}}{\rho_{a1}}\,|\varepsilon_{a1}|\,\hat{v}_{a1} + \frac{|\varepsilon_{a1}|}{\rho_{a1}}\left|\frac{\dot{\rho}_{a1}}{\rho_{a1}}\,e_\phi\right| - \frac{k_{a1}\,a_{a1}}{\eta_{a1}}\,\tilde{v}_{a1}\,\dot{\hat{v}}_{a1} \\
&\leq -\lambda_1\,p_{a1}\,\varepsilon_{a1}^2 - k_{a1}\,p_{a1}\,|\varepsilon_{a1}|\,\hat{v}_{a1} + R_{a1}\,|\varepsilon_{a1}| - \frac{k_{a1}\,a_{a1}}{\eta_{a1}}\,\tilde{v}_{a1}\,\dot{\hat{v}}_{a1}
\end{aligned}
\tag{22}
$$

where $p_{a1} = \frac{1}{\rho_{a1}}$, $R_{a1} = \frac{1}{\rho_{a1}}\left|\frac{\dot{\rho}_{a1}}{\rho_{a1}}\,e_\phi\right|$, because $|\xi_{a1}| \leq 1$ and $\rho_{a1}, \dot{\rho}_{a1}$ are bounded variables and the former is always greater than zero and the latter is always less than zero, then it follows that

$$
0 < p_{al1} \leq p_{a1} \leq p_{ah1},\, 0 < R_{al1} \leq R_{a1} \leq R_{ah1}
\tag{23}
$$

Therefore, the expression of $\dot{V}_{a1}$ is rewritten as

$$
\dot{V}_{a1} \leq -\lambda_{a1}\,p_{al1}\,\varepsilon_{a1}^2
\tag{24}
$$

where $\tilde{v}_{a1} = \frac{R_{ah1}}{p_{al1} k_{a1}}, a_{a1} = p_{al1}$. Integrating $\dot{V}_{a1}$ over the time range $[0, t]$ one has that $V_{a1}(t) + \int_0^t \lambda_{a1} p_{al1} \varepsilon_{a1}^2 d\tau \leq V_{a1}(0)$ that is, $\forall t \in [0, T]$ it means:

$$\frac{1}{2} \log\left(\frac{1}{1 - \xi_{a1}^2}\right) \leq V_{a1} \leq V_{a1}(0) = \bar{\sigma}_{a1} \tag{25}$$

$$\frac{k_{a1} a_{a1}}{2 \eta_{a1}} \tilde{v}_{a1}^2 \leq V_{a1} \leq V_{a1}(0) = \bar{\sigma}_{a1} \tag{26}$$

According to (25) and (26), we know that: $|\xi_{a1}| < \sqrt{1 - e^{\bar{\sigma}_{a1}}} < 1$ and $|\hat{v}_{a1}| \leq \sqrt{\frac{2 \eta_{a1} \bar{\sigma}_{a1}}{k_{a1} a_{a1}}} + v_{a1}$ are established for all $t \in [0, T]$.

Next, for the θ, ψ component in the vector, the Lyapunov function is selected as

$$V_{ai} = \frac{1}{2} \log\left(\frac{1}{1 - \xi_{ai}^2}\right) + \frac{k_{ai} a_{ai}}{2 \eta_{ai}} \tilde{v}_{ai}^2, i = 2, 3 \tag{27}$$

where $\tilde{v}_{ai} = v_{ai} - \hat{v}_{ai}$, a_{ai} is an unknown constant, and the derivation process is similar to (21).

$$\dot{V}_{ai} = \frac{\varepsilon_{ai}}{\rho_{ai}}\left(\dot{e}_q - \frac{\dot{\rho}_{ai}}{\rho_{ai}} e_q\right) - \frac{k_{ai} a_{ai}}{\eta_{ai}} \tilde{v}_{ai} \dot{\hat{v}}_{ai}, i = 2, 3; q = \theta, \psi \tag{28}$$

For the e_θ, e_ψ component in the vector, define an extraction vector: $b_i, i = 2, 3, i$ means that the element at position i in the vector b is equal to 1 and the elements at the remaining positions are 0, used to extract the quantity of e_θ, e_ψ active channels in the system model. According to (13) and (15) we have that

$$\begin{aligned}
\dot{V}_{ai} &= \frac{\varepsilon_{ai}}{\rho_{ai}}\left(b_{ai}(G_a \Gamma_a) - \frac{\dot{\rho}_{ai}}{\rho_{ai}} e_q\right) - \frac{k_{ai} a_{ai}}{\eta_{ai}} \tilde{v}_{ai} \dot{\hat{v}}_{ai} \\
&= \frac{\varepsilon_{ai}}{\rho_{ai}}\left(-\lambda_{ai} \varepsilon_{ai} - \text{sgn}(\varepsilon_{ai}) k_{ai} \hat{v}_{ai} - \frac{\dot{\rho}_{ai}}{\rho_{ai}} e_q\right) - \frac{k_{ai} a_{ai}}{\eta_{ai}} \tilde{v}_{ai} \dot{\hat{v}}_{ai} \\
&\leq -\frac{\lambda_{ai}}{\rho_{ai}} \varepsilon_{ai}^2 - \frac{k_{ai}}{\rho_{ai}} |\varepsilon_{ai}| \hat{v}_{ai} + \frac{|\varepsilon_{ai}|}{\rho_i}\left|\frac{\dot{\rho}_{ai}}{\rho_{ai}} e_q\right| - \frac{k_{ai} a_{ai}}{\eta_{ai}} \tilde{v}_{ai} \dot{\hat{v}}_{ai} \\
&\leq -\lambda_{ai} p_{ai} \varepsilon_{ai}^2 - k_{ai} p_{ai} |\varepsilon_{ai}| \hat{v}_{ai} + R_{ai} |\varepsilon_{ai}| - \frac{k_{ai} a_{ai}}{\eta_{ai}} \tilde{v}_{ai} \dot{\hat{v}}_{ai}
\end{aligned} \tag{29}$$

where $p_{ai} = \frac{1}{\rho_{ai}}, R_{ai} = \frac{1}{\rho_{ai}}\left|\frac{\dot{\rho}_{ai}}{\rho_{ai}} e_\phi\right|$. Since $|\xi_{ai}| \leq 1$ and $\rho_{ai}, \dot{\rho}_{ai}$ are bounded variables and the former is always greater than zero and the latter is always less than zero, which leads to:

$$0 < p_{ali} \leq p_{ai} \leq p_{ahi}, 0 < R_{ali} \leq R_{ai} \leq R_{ahi} \tag{30}$$

Therefore, the expression of $\dot{V}_{ai}$ is:

$$\dot{V}_{ai} \leq -\lambda_{ai} p_{ali} \varepsilon_{ai}^2 \tag{31}$$

where $\tilde{v}_{ai} = \frac{R_{ahi}}{p_{ali} k_{ai}}, a_{ai} = p_{ali}$, integrating $\dot{V}_{ai}$ over the time range $[0, t]$ one has: $V_{ai}(t) + \int_0^t \lambda_{ai} p_{ali} \varepsilon_{ai}^2 d\tau \leq V_{ai}(0)$ that is, $\forall t \in [0, T]$ it means:

$$\frac{1}{2} \log\left(\frac{1}{1 - \xi_{ai}^2}\right) \leq V_{ai} \leq V_{ai}(0) = \bar{\sigma}_{ai} \tag{32}$$

$$\frac{k_{ai} a_{ai}}{2 \eta_{ai}} \tilde{v}_{ai}^2 \leq V_{ai} \leq V_{ai}(0) = \bar{\sigma}_{ai} \tag{33}$$

According to Equations (32) and (33), we know that: $|\xi_{ai}| < \sqrt{1 - e^{\bar{\sigma}_{ai}}} < 1$ and $|\hat{v}_{ai}| \leq \sqrt{\frac{2\eta_{ai}\bar{\sigma}_{ai}}{k_{ai}a_{ai}}} + v_{ai}$ are established for all $t \in [0, T]$.

Finally, let us select the Lyapunov function as

$$V_{ui} = \frac{1}{2}\log\left(\frac{1}{1 - \xi_{ui}^2}\right) + \frac{k_{ui}a_{ui}}{2\eta_{ui}}\tilde{v}_{ui}^2, i = 1, 2, 3 \tag{34}$$

where $\tilde{v}_{ui} = v_{ui} - \hat{v}_{ui}$, a_{ui} is an unknown constant, and the derivation process is similar to (21). Then it follows that:

$$\dot{V}_{ui} = \frac{\varepsilon_{ui}}{\rho_{ui}}\left(\dot{e}_u - \frac{\dot{\rho}_{ui}}{\rho_{ui}}e_u\right) - \frac{k_{ui}a_{ui}}{\eta_{ui}}\tilde{v}_{ui}\dot{\hat{v}}_{ui}, i = 1, 2, 3; u = \omega_x, \omega_y, \omega_z \tag{35}$$

Define an extraction vector: $b_i, i = 1, 2, 3$, i means that the element at position i in the vector b is equal to 1 and the elements at the remaining positions are 0, used to extract the quantity of $e_{\omega_x}, e_{\omega_y}, e_{\omega_z}$ active channels in the system model. According to the expression of (14) and (16) one has that

$$\begin{aligned}
\dot{V}_{ui} &= \frac{\varepsilon_{ui}}{\rho_{ui}}\left(b_i I_0^{-1}Mg + b_i(I_0^{-1}u_v) - \dot{\delta}_i - \frac{\dot{\rho}_{ui}}{\rho_{ui}}e_u + d_i\right) - \frac{k_{ui}a_{ui}}{\eta_{ui}}\tilde{v}_{ui}\dot{\hat{v}}_{ui} \\
&= \frac{\varepsilon_{ui}}{\rho_{ui}}\left(\frac{6}{ml^2}Mg_i - \lambda_{ui}\varepsilon_{ui} - \text{sgn}(\varepsilon_{ui})k_{ui}\hat{v}_{ui} - \frac{\dot{\rho}_{ui}}{\rho_{ui}}e_u - \dot{\delta}_i + d_i\right) - \frac{k_{ui}a_{ui}}{\eta_{ui}}\tilde{v}_{ui}\dot{\hat{v}}_{ui} \\
&\leq -\frac{\lambda_{ui}}{\rho_{ui}}\varepsilon_{ui}^2 - \frac{k_{ui}}{\rho_{ui}}|\varepsilon_{ui}|\hat{v}_{ui} + \frac{|\varepsilon_{ui}|}{\rho_{ui}}\left|\frac{6}{ml^2}Mg_1 - \frac{\dot{\rho}_{ui}}{\rho_{ui}}e_u - \dot{\delta}_i + d_i\right| - \frac{k_{ui}a_{ui}}{\eta_{ui}}\tilde{v}_{ui}\dot{\hat{v}}_{ui} \\
&\leq -\lambda_{ui}p_{ui}\varepsilon_{ui}^2 - k_{ui}p_{ui}|\varepsilon_{ui}|\hat{v}_{ui} + R_{ui}|\varepsilon_{ui}| - \frac{k_{ui}a_{ui}}{\eta_{ui}}\tilde{v}_{ui}\dot{\hat{v}}_{ui}
\end{aligned} \tag{36}$$

where $p_{ui} = \frac{1}{\rho_{ui}}$, $R_{ui} = \frac{1}{\rho_{ui}}\left|\frac{6}{ml^2}Mg_i - \dot{\delta}_i - \frac{\dot{\rho}_{ui}}{\rho_{ui}}e_u + d_i\right|$, because $|\xi_{ui}| \leq 1$ and $\rho_{ui}, \dot{\rho}_{ui}$, $\frac{6}{ml^2}Mg_i, \dot{\delta}_i$ are bounded variables, which leads to:

$$0 < p_{uli} \leq p_{ui} \leq p_{uhi}, 0 < R_{uli} \leq R_{ui} \leq R_{uhi} \tag{37}$$

Therefore, the expression of $\dot{V}_{ui}$ is:

$$\dot{V}_{ui} \leq -\lambda_{ui}p_{uli}\varepsilon_{ui}^2 \tag{38}$$

where $\tilde{v}_{ui} = \frac{R_{uhi}}{p_{uli}k_{ui}}$, $a_{ui} = p_{uli}$, Integrating $\dot{V}_{ui}$ over the time range $[0, t]$ one has:

$$V_{ui}(t) + \int_0^t \lambda_{ui}p_{uli}\varepsilon_{ui}^2 d\tau \leq V_{ui}(0) \tag{39}$$

that is, for $\forall t \in [0, T]$ it means:

$$\frac{1}{2}\log\left(\frac{1}{1 - \xi_{ui}^2}\right) \leq V_{ui} \leq V_{ui}(0) = \bar{\sigma}_{ui} \tag{40}$$

$$\frac{k_{ai}a_{ai}}{2\eta_{ai}}\tilde{v}_{ui}^2 \leq V_{ui} \leq V_{ui}(0) = \bar{\sigma}_{ui} \tag{41}$$

According to Equations (40) and (41), we know that: $|\xi_{ui}| < \sqrt{1 - e^{\bar{\sigma}_{ui}}} < 1$ and $|\hat{v}_{ui}| \leq \sqrt{\frac{2\eta_{ui}\bar{\sigma}_{ui}}{k_{ui}a_{ui}}} + v_{ui}$ are established for all $t \in [0, T]$. It is deduced by contradiction that $T = +\infty$, that is $\left|\xi_j\right| < 1 (j = a1, a2, a3, u1, u2, u3)$ for all $t \in [0, +\infty)$. Moreover, it is deduced from (15) and Equation (16), $\hat{v}_j$ is bounded.

According to (31), (34) and (39) that ε_j is bounded. By applying Barbalat's lemma, it is deduced that $\lim_{t\to\infty} \varepsilon_j = 0$ that is $\lim_{t\to\infty} \xi_j = 0$ and $\lim_{t\to\infty} e_j = 0$. In summary, the tracking errors converge to zero asymptotically and meets the preset dynamic performance requirements, and the proof is completed. □

4.3. Parameters Tuning

The control law represented by (15), (16) consists of the conversion error ε_i, $(i = a, u)$, the estimate of the adaptive parameter $\hat{v}_i$, and the control parameters λ_i, k_i, η_i. In this section, the role and effects of the various parameters involved in the control law are explained. The positive constant λ_i is the gain coefficient of ε_i, which responds to the response of the input signal to the previous state error or the tracking error. If the value of λ_i is increased, the feedback of the control input to the error becomes larger accordingly. λ_i is worth a reasonable increase to accelerate the convergence of the error, but if the value of λ_i is too large, it will lead to an increase in the amount of overshoot and even lead to error overshoot causing system instability. If the λ_i value is too small, it may cause insufficient control input leading to system instability. Then the positive constant k_i and η_i are the gain coefficient of the adaptive parameter $\hat{v}_i$ and its derivative $\dot{\hat{v}}_i$. The value of k_i reflects the effect of the adaptive parameter on the control input, and η_i determines the rate of change of the adaptive parameter. The main role of the adaptive parameter is to regulate the steady-state error of the system and to make the system asymptotically stable. The values of k_i and η_i reflect the effect of the adaptive parameter on the error for compensation. Therefore, improving the steady-state performance of the system, i.e., accelerating the convergence of the steady-state error within a certain time, is the main function of the adaptive parameters.

As mentioned above, the three parameters λ_i, k_i, η_i play the role of regulating the speed of error convergence, the steady-state error, and the variation of the adaptive parameters. In the boundary function, the three values ρ_{i0}, l_i, $\rho_{i\infty}$ are the initial value of the boundary function, the convergence rate of the function, and the final convergence boundary that is the final value. The design of the three parameters constrains the trend and the range of the state error, and the existence of the boundary function is the main reason for the selection of APPC in this paper, and the angular velocity constraint in the special environment of the asteroid is achieved by designing the boundary function.

5. Simulation Results

The simulations are divided into four parts. The first subsection shows the simulation results for the Cubli Rovers on Earth and the second part demonstrates the effectiveness of the proposed control method for the environment on the asteroid. The third section shows the effect of changes in each parameter of the APPC controller on the control performance. In the last part, the method in this paper compares the Backstepping method [37] and the PD control method and provides the comparison results and discussion to show that the APPC method can make the system reach the steady state well, and shows good control performance in the control process, which can be well adapted to the requirements of the asteroid microgravity environment. Thus, it is demonstrated that the proposed method in this paper is superior to the Backstepping method and PD control method.

5.1. Simulation Results and Discussion on Earth

The target attitude angle is all $\phi = \theta = \psi = 0$, The initial angular velocity of Cubli Rovers is $\omega_x = \omega_y = \omega_z = 0$. The initial attitude angle is set to $\phi = -0.3$ rad, $\theta = 0.3$ rad, $\psi = 0.3$ rad. Gravitational acceleration $g = 9.8$ m/s^2, total mass is 2 kg, cube side length is $l = 0.2$ m. The values of performance boundary functions and control parameters in the simulation are shown in the following Table 1.

Table 1. Simulation Parameter Settings.

λ_i	$\lambda_{a1} = 0.55,\ \lambda_{a2} = 0.55,\ \lambda_{a3} = 0.55$ $\lambda_{u1} = 0.55,\ \lambda_{u2} = 0.55,\ \lambda_{u3} = 0.55$
k_i	$k_{a1} = 0.01,\ k_{a2} = 0.01,\ k_{a3} = 0.01$ $k_{u1} = 0.01,\ k_{u2} = 0.01,\ k_{u3} = 0.01$
η_i	$\eta_{a1} = 0.0053,\ \eta_{a2} = 0.0053,\ \eta_{a3} = 0.0053$ $\eta_{u1} = 0.0053,\ \eta_{u2} = 0.0053,\ \eta_{u3} = 0.0053$
ρ_{i0}	$\rho_{a10} = 0.5,\ \rho_{a20} = 0.5,\ \rho_{a30} = 0.5$ $\rho_{u10} = 0.9,\ \rho_{u20} = 0.9,\ \rho_{u30} = 0.9$
$\rho_{i\infty}$	$\rho_{a1\infty} = 0.008,\ \rho_{a2\infty} = 0.008,\ \rho_{a3\infty} = 0.008$ $\rho_{u1\infty} = 0.08,\ \rho_{u2\infty} = 0.08,\ \rho_{u3\infty} = 0.08$
l_i	$l_{a1} = -2,\ l_{a2} = -2,\ l_{a3} = -2$ $l_{u1} = -2,\ l_{u2} = -2,\ l_{u3} = -2$

Figures 5–7 show that the dynamic change curve of the attitude angle in the process, which is also the dynamic performance of the attitude angle error. It can be seen that the attitude angle tracking error has always been within the prescribed performance range of the boundary function. When $t \rightarrow +\infty$, e_ϕ, e_θ, e_ψ, successfully converged to zero, ensuring that the key indicators of steady-state error and convergence rate in the prescribed performance function. As seen in Figures 8–10, it can also be seen that the three-axis angular velocity variation curves during the control process. As seen in Figures 11–13, it can be seen that the tracking error is always within the prescribed performance range of the boundary function, which meets the requirements of the control rate. As seen in Figures 14–16, it reflects the input value of the entire system, that is, the input torque generated by the flywheel. It can be seen from its peak value and time that it meets the actual flywheel operating conditions.
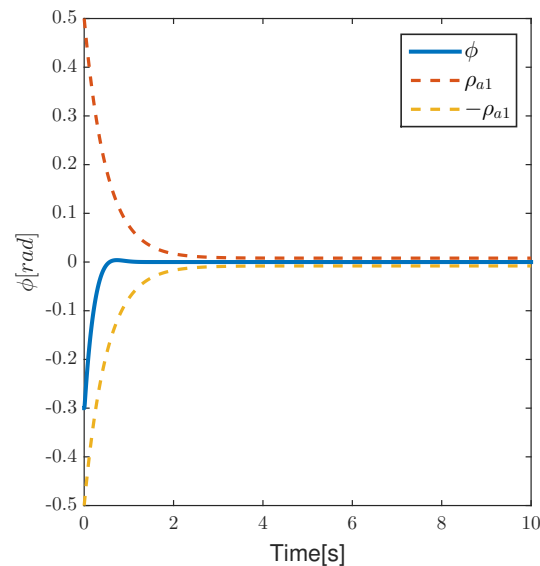
Figure 5. Curve of roll angle ϕ.
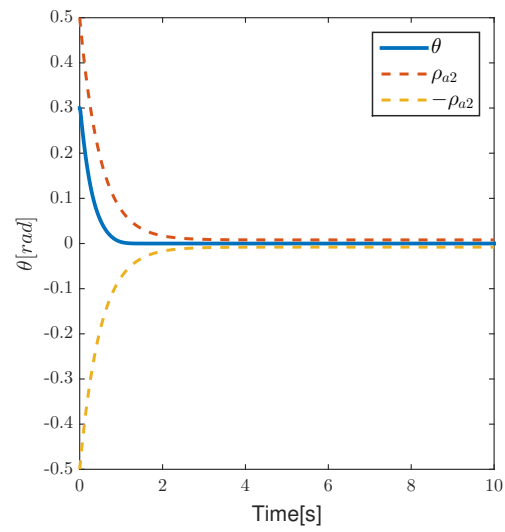
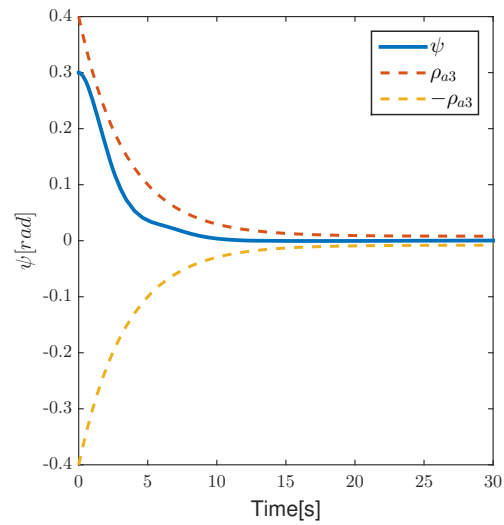**Figure 6.** Curve of yaw angle θ.
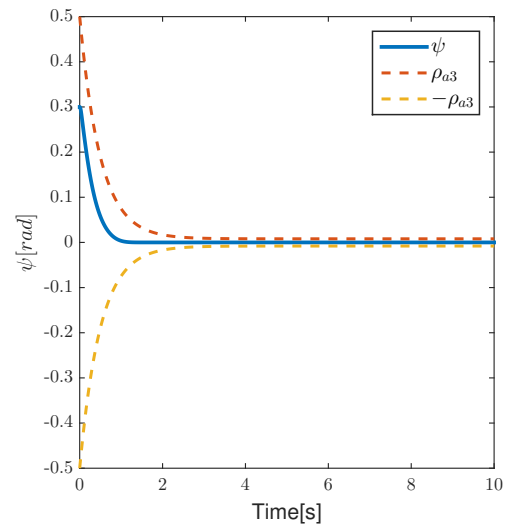

Figure 7. Curve of pitch angle ψ.
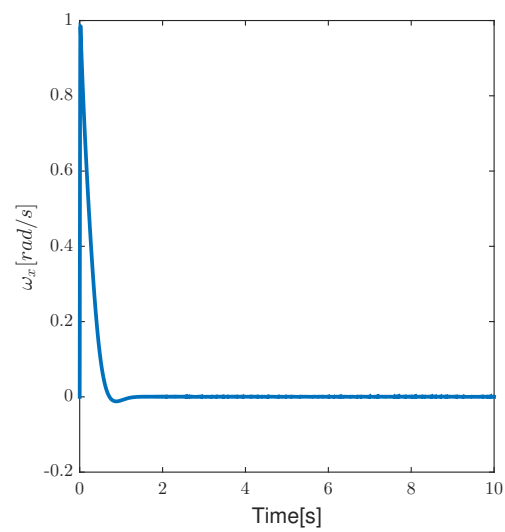
**Figure 8.** Curve of roll rate ω_x.
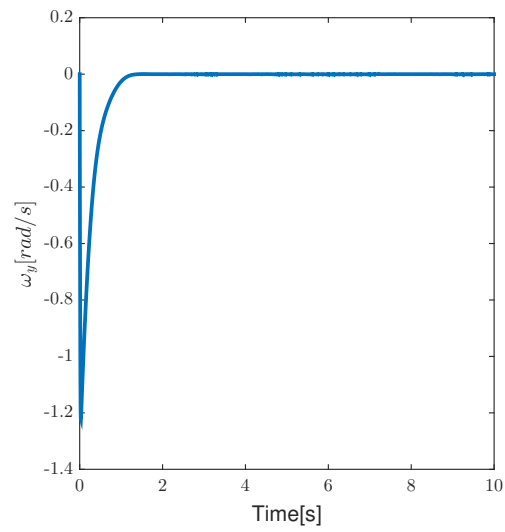
**Figure 9.** Curve of yaw rate ω_y.
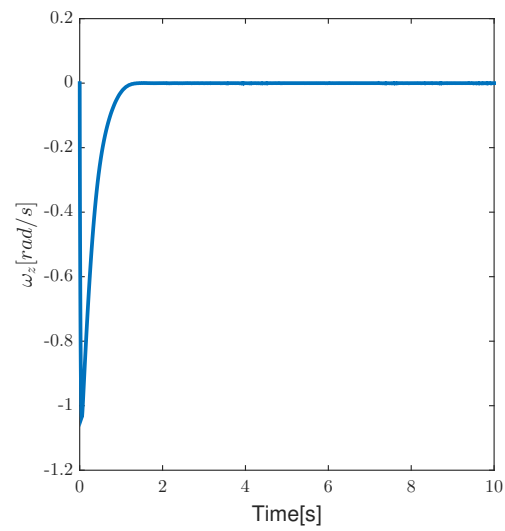
**Figure 10.** Curve of pitch rate ω_z.
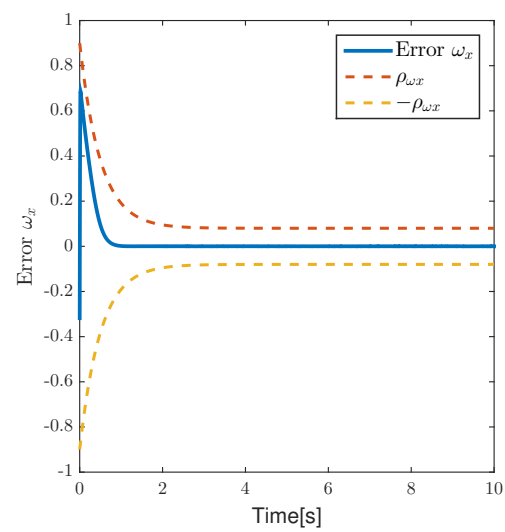
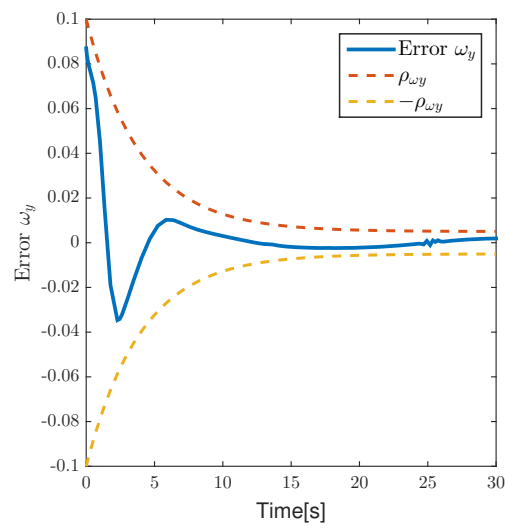**Figure 11.** Curve of error $e_{\omega x}$.
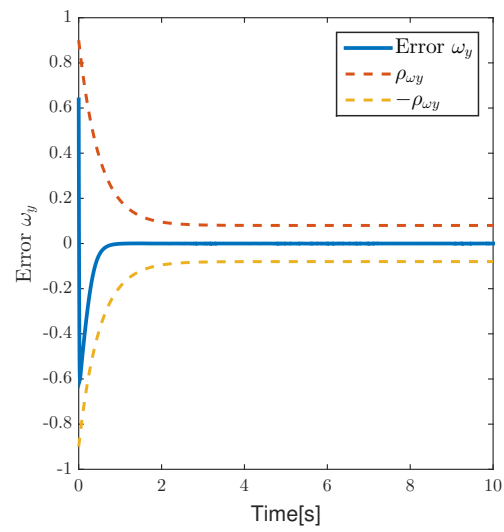
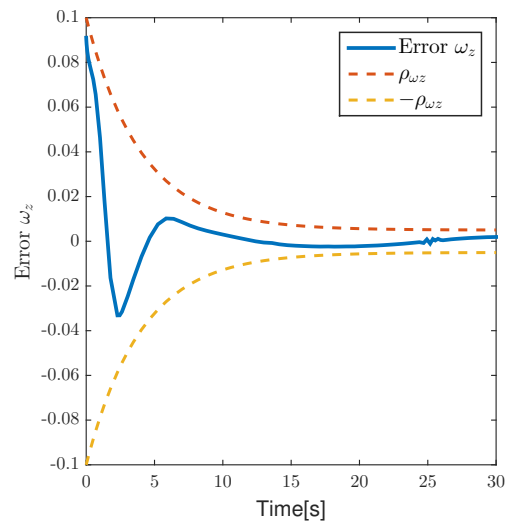**Figure 12.** Curve of error $e_{\omega y}$.
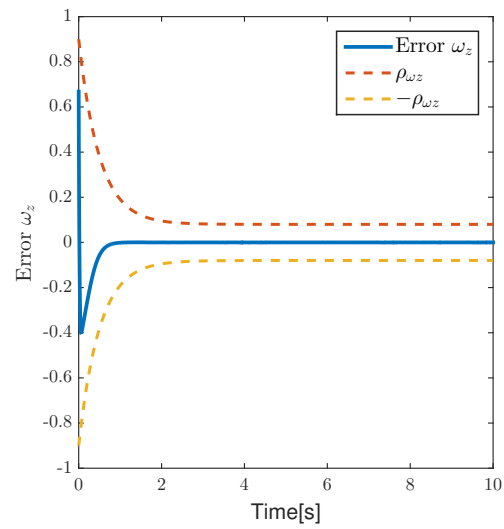

Figure 13. Curve of error $e_{\omega z}$.
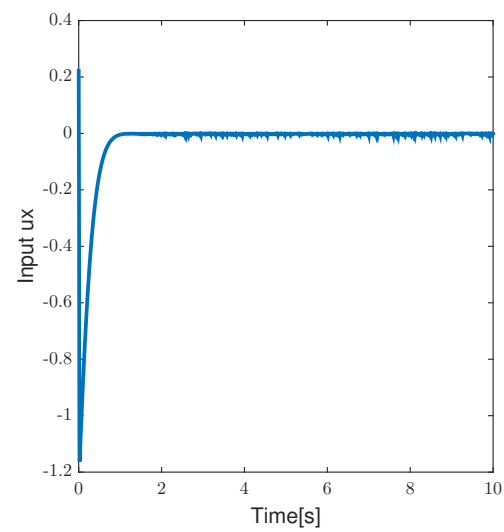
Figure 14. Curve of control input u_x.
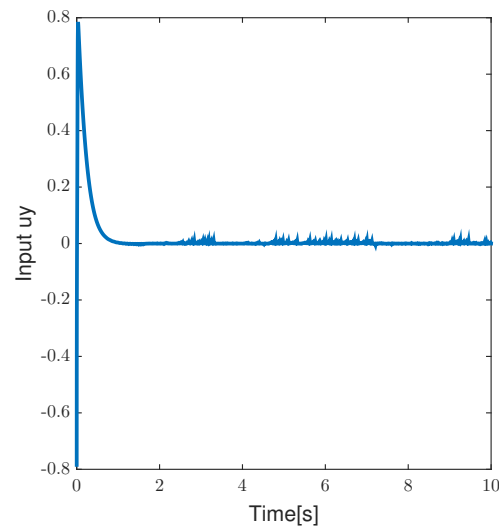
Figure 15. Curve of control input u_y.
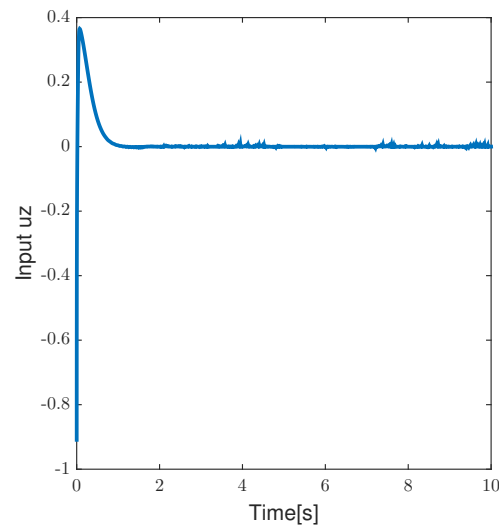
Figure 16. Curve of control input u_z.

5.2. Simulation Results and Discussion in Asteroid Environment

The target attitude angle is all $\phi = \theta = \psi = 0$, The initial angular velocity of Cubli Rovers is $\omega_x = \omega_y = \omega_z = 0$. The initial attitude angle is set to $\phi = -0.3$ rad, $\theta = 0.3$ rad, $\psi = 0.3$ rad. Gravitational acceleration $g = 0.002$ m/ s^2, total mass is 2 kg, cube side length is $l = 0.2$ m, The values of performance boundary functions and control parameters in the simulation are shown in the following Table 2.

The external disturbance values are as follows:

$$d = \begin{bmatrix} d_x \\ d_y \\ d_z \end{bmatrix} = \begin{bmatrix} 0.02\sin(\omega t) \\ 0.02\sin(\omega t) \\ 0.02\sin(\omega t) \end{bmatrix} \tag{42}$$

As seen in Figures 17–28, it has been verified by simulation results that it is possible to ensure self-equilibrium stability without leaving the surface of the asteroid through the prescribed performance design. Meanwhile, it can be seen from the figures that in the presence of external disturbances, the control method designed in this paper can well resist external disturbances and ensure that the attitude angle is stable near the steady

state. Periodic chattering exists in the input to ensure anti-interference and make the system robust.

Table 2. Simulation Parameter Settings.

λ_i	$\lambda_{a1} = 0.041, \ \lambda_{a2} = 0.041, \ \lambda_{a3} = 0.041$ $\lambda_{u1} = 0.041, \ \lambda_{u2} = 0.041, \ \lambda_{u3} = 0.041$
k_i	$k_{a1} = 0.01, \ k_{a2} = 0.01, \ k_{a3} = 0.01$ $k_{u1} = 0.01, \ k_{u2} = 0.01, \ k_{u3} = 0.01$
η_i	$\eta_{a1} = 0.0053, \ \eta_{a2} = 0.0053, \ \eta_{a3} = 0.0053$ $\eta_{u1} = 0.005, \ \eta_{u2} = 0.005, \ \eta_{u3} = 0.005$
ρ_{i0}	$\rho_{a10} = 0.4, \ \rho_{a20} = 0.4, \ \rho_{a30} = 0.4$ $\rho_{u10} = 0.1, \ \rho_{u20} = 0.1, \ \rho_{u30} = 0.1$
$\rho_{i\infty}$	$\rho_{a1\infty} = 0.008, \ \rho_{a2\infty} = 0.008, \ \rho_{a3\infty} = 0.008$ $\rho_{u1\infty} = 0.005, \ \rho_{u2\infty} = 0.005, \ \rho_{u3\infty} = 0.005$
l_i	$l_{a1} = -0.29, \ l_{a2} = -0.29, \ l_{a3} = -0.29$ $l_{u1} = -0.25, \ l_{u2} = -0.25, \ l_{u3} = -0.25$
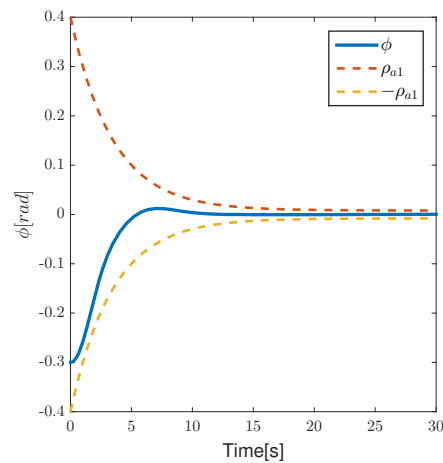
Figure 17. Curve of roll angle ϕ.
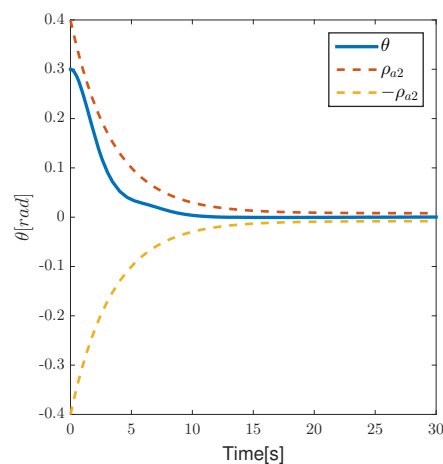
Figure 18. Curve of yaw angle θ.

Figure 19. Curve of pitch angle ψ.
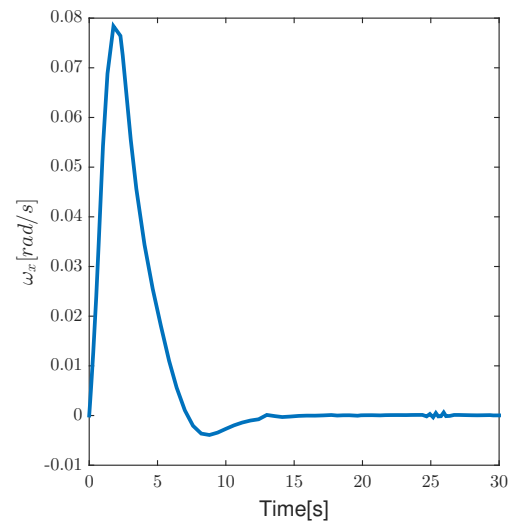
Figure 20. Curve of roll rate ω_x.
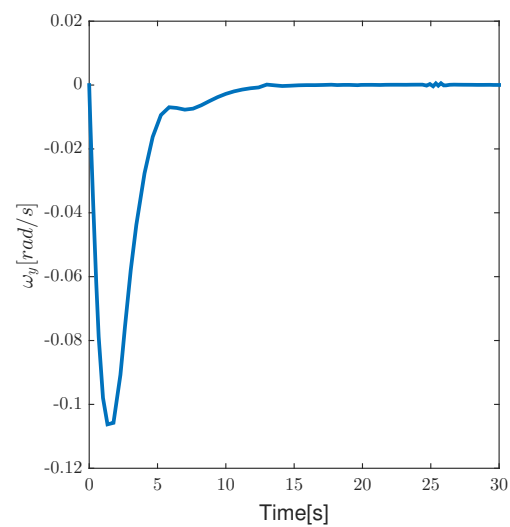
Figure 21. Curve of yaw rate ω_y.
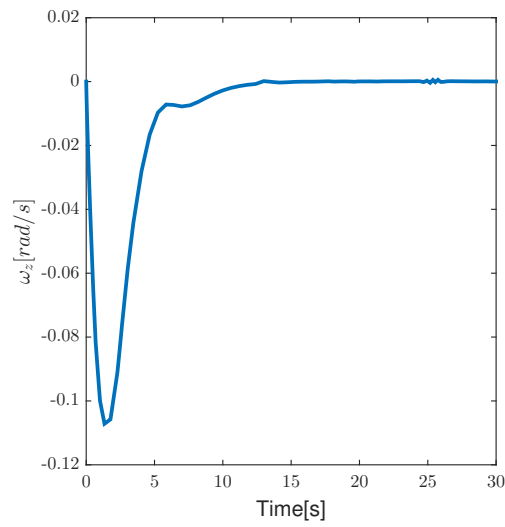
Figure 22. Curve of pitch rate ω_z.
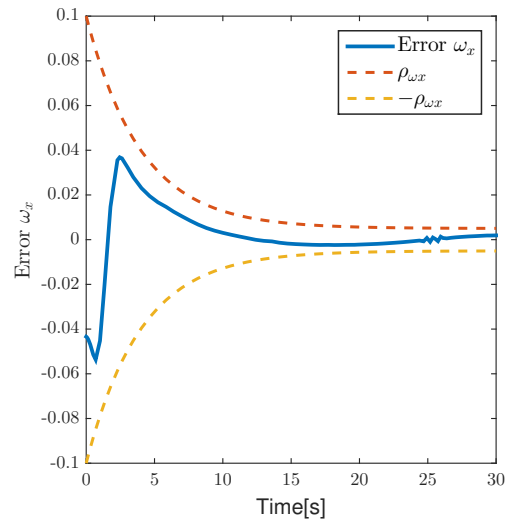
Figure 23. Curve of error $e_{\omega x}$.

Figure 24. Curve of error $e_{\omega y}$.

Figure 25. Curve of error $e_{\omega z}$.
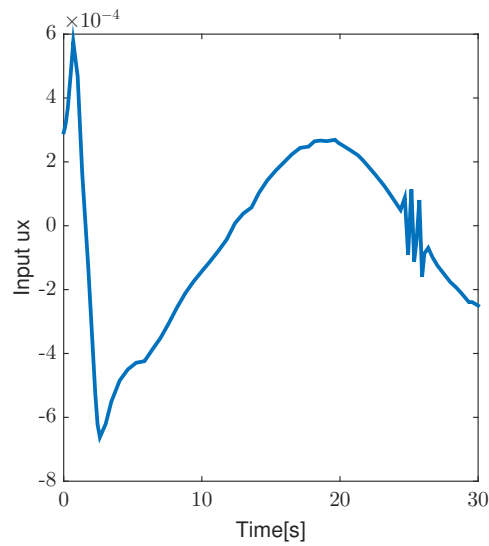
Figure 26. Curve of control input u_x.
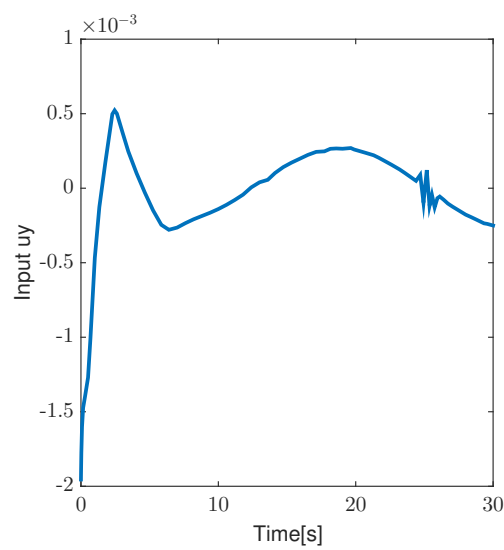
Figure 27. Curve of control input u_y.
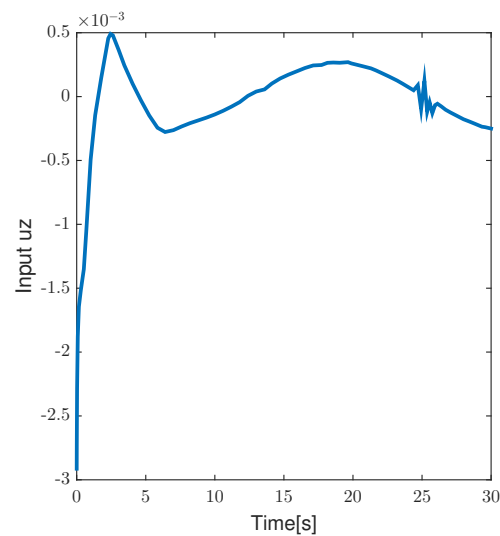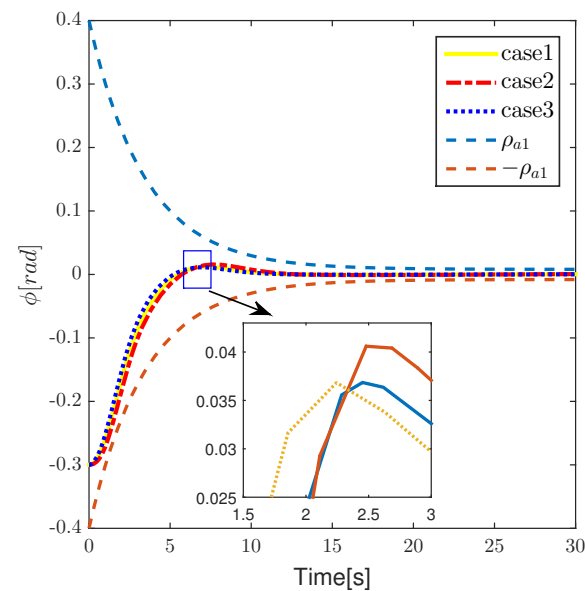
Figure 28. Curve of control input u_z.

5.3. Performance Comparison Results for Different Control Parameters

(1) Figures 29–32 show that the influence of controller parameters λ_i, k_i, η_i. No change in performance boundary function. Three groups of parameters are selected:

Case1: $\lambda_i = diag(0.041, 0.041, 0.041)$, $k_i = diag(0.01, 0.01, 0.01)$, $\eta_a = diag(0.0053, 0.0053, 0.0053)$, $\eta_u = diag(0.005, 0.005, 0.005)$.

Case2: $\lambda_i = diag(0.029, 0.029, 0.029)$, $k_i = diag(0.01, 0.01, 0.01)$, $\eta_i = diag(0.0035, 0.0035, 0.0035)$.

Case3: $\lambda_i = diag(0.046, 0.046, 0.046)$, $k_i = diag(0.01, 0.01, 0.01)$, $\eta_i = diag(0.006, 0.006, 0.006)$.

Figure 29. Curve of roll angle ϕ under different control parameters.
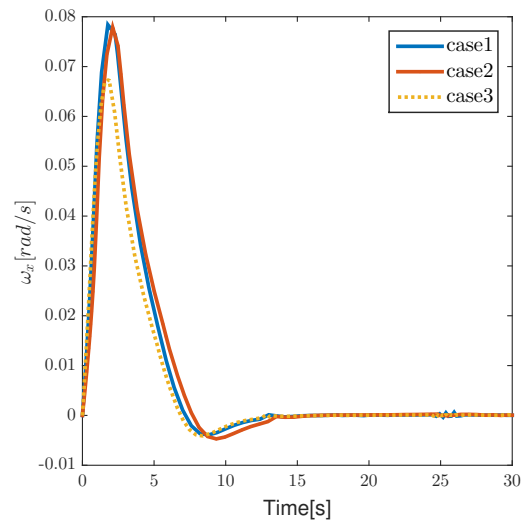
Figure 30. Curve of roll rate ω_x under different control parameters.
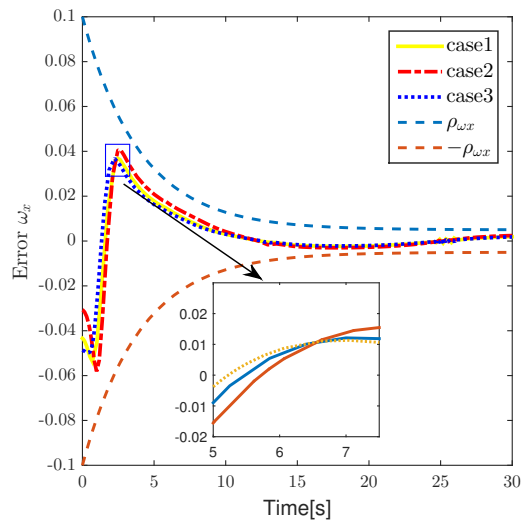
Figure 31. Curve of error $e_{\omega x}$ under different control parameters.
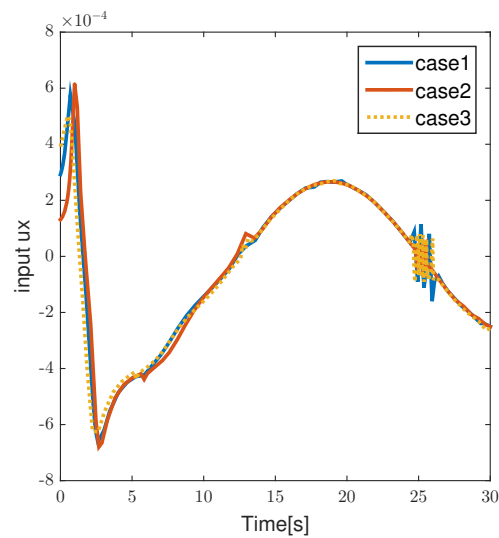

Figure 32. Curve of control input u_x under different control parameters.

(2) Figures 33–36 show that the influence of boundary performance function:

Case1: $\rho_{ai0} = 0.4$, $\rho_{ai\infty} = 0.008$, $l_{ai} = -0.29$, $\rho_{ui0} = 0.1$, $\rho_{ui\infty} = 0.005$, $l_{ui} = -0.25$
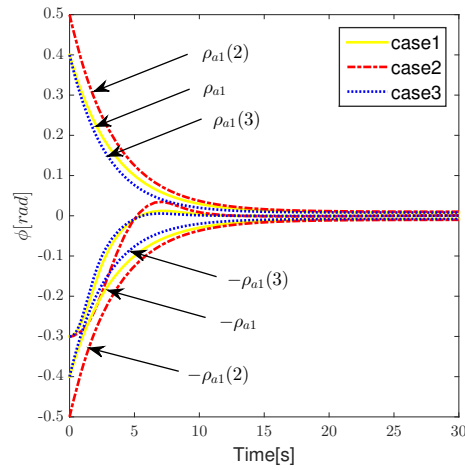Case2: $\rho_{ai0} = 0.5$, $\rho_{ai\infty} = 0.01$, $l_{ai} = -0.29$, $\rho_{ui0} = 0.2$, $\rho_{ui\infty} = 0.01$, $l_{ui} = -0.25$
Case3: $\rho_{ai0} = 0.4$, $\rho_{ai\infty} = 0.008$, $l_{ai} = -0.35$, $\rho_{ui0} = 0.1$, $\rho_{ui\infty} = 0.005$, $l_{ui} = -0.35$

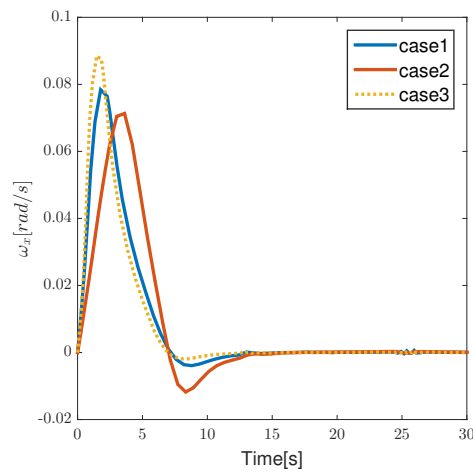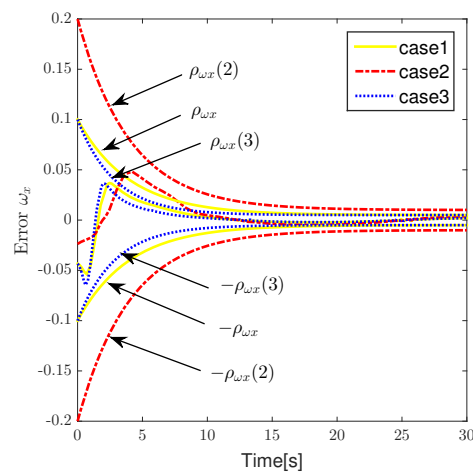**Figure 33.** Curve of roll angle ϕ under different boundary performance function.

Figure 34. Curve of roll rate ω_x under different boundary performance function.
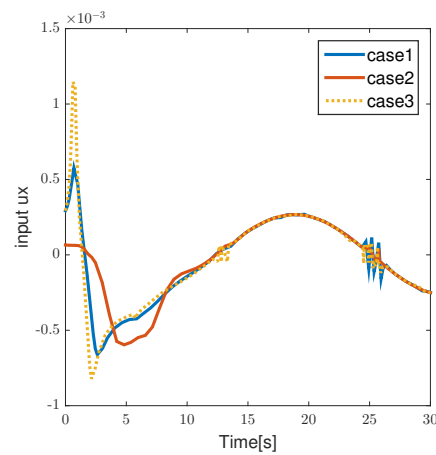

Figure 35. Curve of error $e_{\omega x}$ under different boundary performance function.

Figure 36. Curve of control input u_x under different boundary performance function.

5.4. Comparison Results and Discussion

The method APPC proposed in this paper is compared with the classical PD control and the Backstepping method, and the results are shown in the following Figures 37–43. Furthermore, to assess the Control Effort required by different control methods throughout the process, the following indicator is introduced

$$E = \int_0^t u^2 dt \tag{43}$$
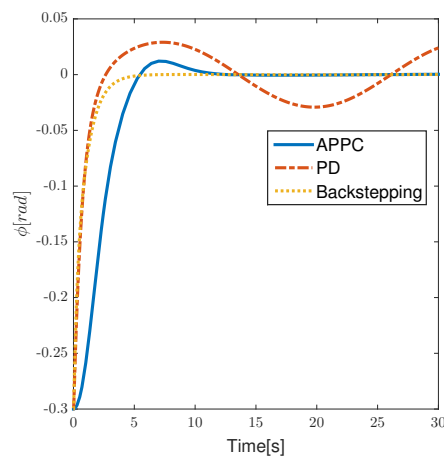
Figure 37. Curve of roll angle ϕ under different control methods.
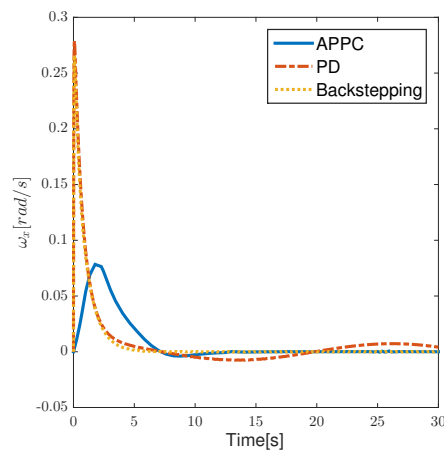
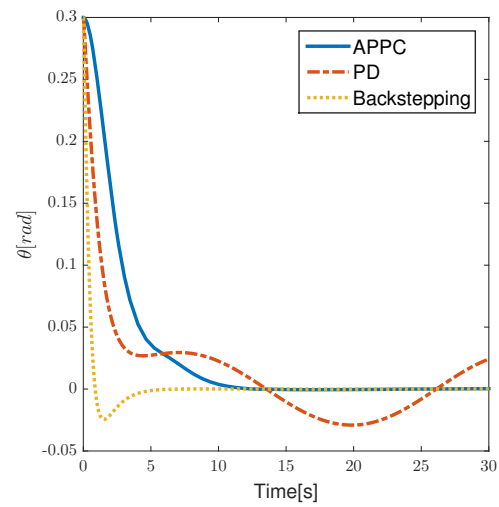**Figure 38.** Curve of roll rate ω_x under different control methods.

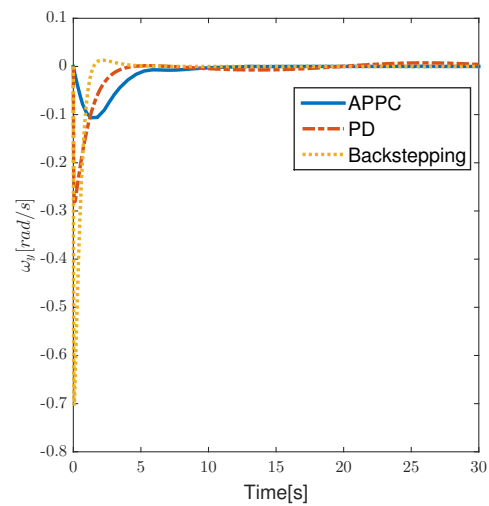**Figure 39.** Curve of yaw angle θ under different control methods.

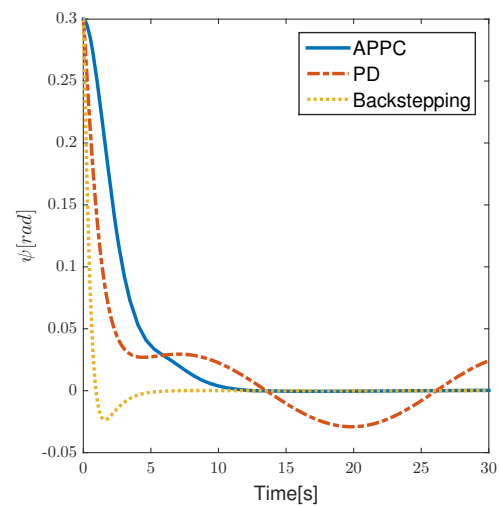**Figure 40.** Curve of yaw rate ω_y under different control methods.

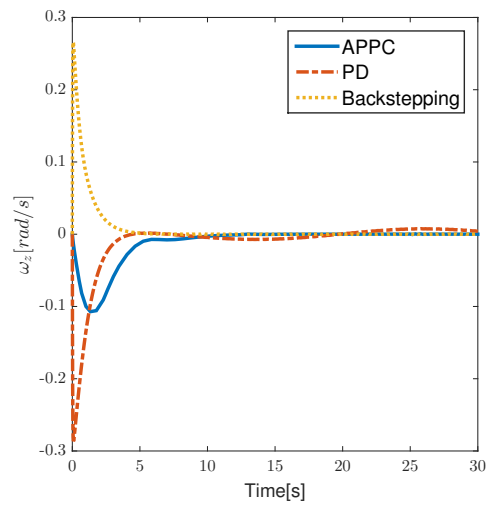**Figure 41.** Curve of pitch angle ψ under different control methods.

Figure 42. Curve of pitch rate ω_z under different control methods.
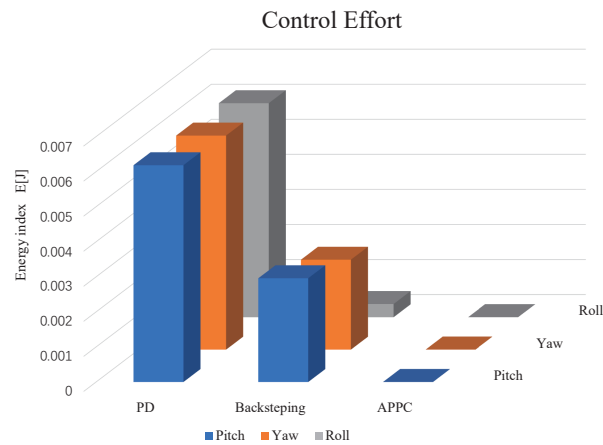

Figure 43. Control effort comparisons under different methods.

The following Figures 44–46 shows the feasibility validation of the three control methods in the case of an asteroid surface:
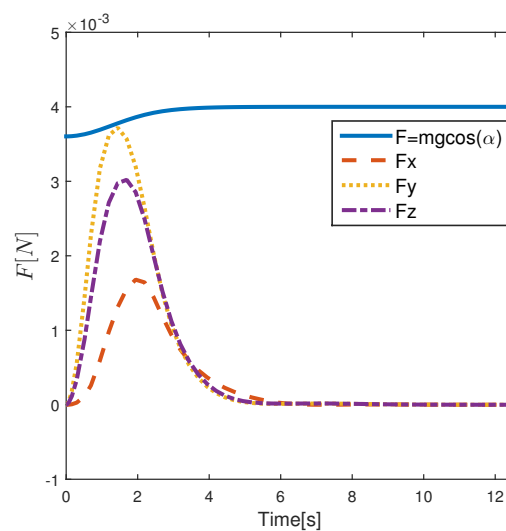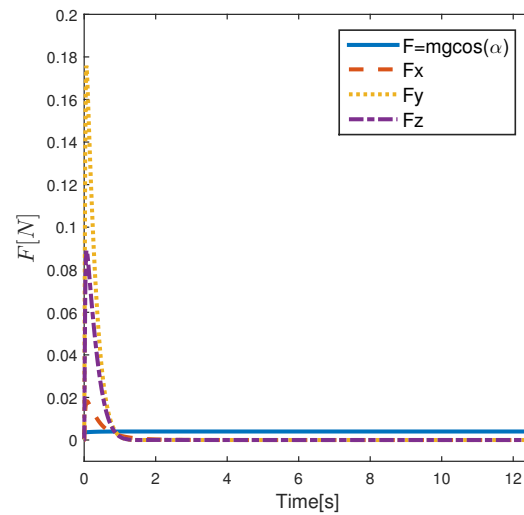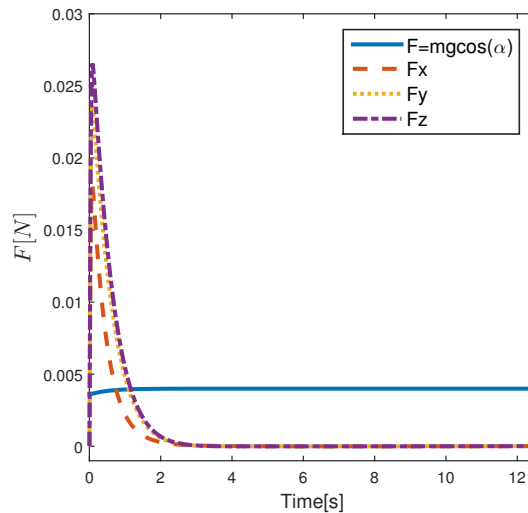

Figure 44. APPC Feasibility Analysis.

Figure 45. Backstepping Feasibility Analysis.

Figure 46. PD Feasibility Analysis

It can be seen in Figures 37–42 that the APPC control method and the Backstepping method [37] can drive the system to a steady state and have a certain anti-disturbance ability. The system under PD control is greatly affected by disturbance so the state quantity changes periodically around the steady state. As seen in Figure 43, APPC can well limit the overshoot, and the energy consumed is the smallest in the whole process.

However, it can be seen from Figures 44–46 that the speed generated by the Backstepping method and the PD method in the control process has exceeded the tolerance, which makes the Cubli Rovers leave the ground and cannot produce self-balancing stabilization behavior. The APPC method proposed in this paper can ensure the normal movement of the system during the control process by designing the boundary function and limiting convergence rate and overshoot. This is also the advantage of the APPC control method for asteroid surfaces proposed in this paper. The value of angular velocity in the control process of the Backstepping method is too large to satisfy the constraint by verification. Because the control effect of the Backstepping method is better in the need for greater angular velocity input which in turn makes the adjustment time shorter and convergence faster. Of course, control effort is also an important part of the reason. In the asteroidal environment, the Cubli Rovers have no energy source, so energy is limited. Control effort is a concern in order to achieve a larger detection area and a longer operating time.

6. Conclusions

The balancing problem of a reaction-wheeled inverted pendulum Cubli Rovers is investigated with consideration of the asteroid weak gravity and avoiding jumping condition. By the presented adaptive prescribed performance control, the tracking errors of the attitude angles and the angle velocity are constrained in the boundary function, and it is proved that asymptotic convergence can be achieved globally. The simulation results demonstrates the effectiveness of the proposed control method. Future work will consider the control of the jump phase of Cubli Rovers, and the control method in terms of jitter vibration in steady state. There is also a further optimization of the performance boundary function to prepare for future balance control problems on uneven ground (more complex ground conditions).

Author Contributions: Conceptualization, H.H.; methodology, Z.L. and Z.G.; software, Z.L.; investigation, Z.L.; resources, H.H., L.S. and H.W.; writing—original draft preparation, Z.L.; writing—review and editing, Z.G. and J.G.; supervision, H.H. All authors have read and agreed to the published version of the manuscript.

Data Availability Statement: Not applicable.

References

1. Fiorini, P.; Burdick, J. The Development of Hopping Capabilities for Small Robots. *Auton. Robot.* **2003**, *14*, 239–254. [CrossRef]
2. Pravec, P.; Harris, A.W. Fast and Slow Rotation of Asteroids. *Icarus* **2000**, *148*, 12–20. [CrossRef]
3. Romain, G.; Laurence, L.; Elisabet, C.; Thierry, M.; Aurelie, M.; Jens, B. MASCOT landing on Asteroid Ryugu: Flight dynamics team contribution to the landing site selection process. In Proceedings of the SpaceOps Conferences, Marseille, France, 28 May–1 June 2018.
4. Dante, A.; Bolatti, B.; Anton, H.J. Quantification of attitude effects on orbital dynamics near asteroids. *Acta Astronaut.* **2020**, *167*, 467–482
5. Shota, K.; Yuichi, T.; Makoto, Y.; Jun'ichiro, K. Stability Analysis of Coupled Orbit–Attitude Dynamics Around Asteroids Using Finite-Time Lyapunov Exponents. *J. Guid. Control Dyn.* **2019**, *42*, 1289–1305.
6. Kenshiro, O.; McMahon, J.W. *Solar Radiation Pressure–Based Orbit Control with Application to Small-Body Landing*; University of Colorado Boulder: Boulder, CO, USA, 2019.
7. Sagdeev, R.Z.; Zakharov, A.V. Brief history of the Phobos mission. *Nature* **1989**, *341*, 581–585. [CrossRef]
8. Reid, R.G.; Roveda, L.; Nesnas, I.A.; Pavone, M. Contact Dynamics of Internally-Actuated Platforms for the Exploration of Small Solar System Bodies. In Proceedings of the i-SAIRAS, Montreal, QC, Canada, 17–19 June 2014.
9. Gajamohan, M.; Merz, M.; Thommen, I.; D'Andrea, R. The Cubli: A cube that can jump up and balance. In Proceedings of the IEEE/RSJ International Conference on Intelligent Robots and Systems, Algarve, Portugal, 7–12 October 2012; pp. 3722–3727.
10. Chaturvedi, N.A.; McClamroch, N.H.; Bernstein, D.S. Asymptotic Smooth Stabilization of the Inverted 3-D Pendulum. *IEEE Trans. Autom. Control* **2009**, *54*, 1204–1215. [CrossRef]
11. Gajamohan, M.; Muehlebach, M.; Widmer, T.; D'Andrea, R. The Cubli: A reaction wheel based 3D inverted pendulum. In Proceedings of the 2013 European Control Conference (ECC), Zurich, Switzerland, 17–19 July 2013; pp. 268–274.
12. Johannes, M.; Spanlang, F.; Gattringer, H. Mechatronic design of a self-balancing three-dimensional inertia wheel pendulum. *Mechatronics* **2015**, *30*, 1–10.
13. Muehlebach, M.; D'Andrea, R. Nonlinear Analysis and Control of a Reaction-Wheel-Based 3-D Inverted Pendulum. *IEEE Trans. Control Syst. Technol.* **2017**, *25*, 235–246. [CrossRef]
14. Chen, Z.; Ruan, X.; Li, Y. Dynamic modeling of a self-balancing cubical robot. *J. Beijing Univ. Technol.* **2018**, *44*, 376–381.
15. Kim, Y.; Park, J.; Han, S. Balancing the Cubli Frame with LQR-controlled Reaction Wheel. *J. Sens. Sci. Technol.* **2018**, *27*, 165–169.
16. Bobrow, F.; Angelico, B.A.; Martins, F.P.R.; Silva, P.S.P. The Cubli: Modeling and Nonlinear Attitude Control Utilizing Quaternions. *IEEE Access* **2021**, *9*, 122425–122442. [CrossRef]
17. Huang, K.; Li, J.; Zhu, Z.; Yu, B. Adaptive robust control for the corner balancing Cubli system with uncertainties. *Trans. Can. Soc. Mech. Eng.* **2021**, *46*, 236–248.
18. Bechlioulis, C.P.; Rovithakis, G.A. Robust Adaptive Control of Feedback Lineariz-able MIMO Nonlinear Systems With Prescribed Performance. *IEEE Trans. Autom. Control* **2008**, *53*, 2090–2099. [CrossRef]

19. Charalampos, P.; Bechlioulis, C.P.; George, A.; Rovithakis, G.A. Adaptive control with guaranteed transient and steady state tracking error bounds for strict feedback systems. *Automatica* **2009**, *45*, 532–538.

20. Charalampos, P.; Bechlioulis, C.P.; George, A.; Rovithakis, G.A. low-complexity global approximation-free control scheme with prescribed performance for unknown pure feedback systems. *Automatica* **2014**, *50*, 1217–1226.

21. Guo, Z.; Henry, D.; Guo, J.; Wang, Z.; Cieslak, J.; Chang, J. Control for systems with prescribed performance guarantees: An alternative interval theory-based approach. *Automatica* **2022**, *146*, 110642.

22. Guo, Z.; Oliveira, T.R.; Guo, J.; Wang, Z. Performance-guaranteed adaptive asymptotic tracking for nonlinear systems with unknown sign-switching control direction. *IEEE Trans. Autom. Control* **2022**.

23. Stamouli, C.J.; Bechlioulis, C.P.; Kyriakopoulos, K.J. Robust dynamic average consensus with prescribed transient and steady state performance. *Automatica* **2022**, *144*, 110503. [CrossRef]

24. Xiao, Y.; de Ruiter, A.H.J.; Ye, D.; Sun, Z. Attitude Tracking Control for Rigid-Flexible Coupled Spacecraft with Guaranteed Performance Bounds. *J. Guid. Control Dyn.* **2019**, *43*, 327–337. [CrossRef]

25. Guo, J.G.; Gu, X.Y.; Guo, Z.Y. Asymptotic adaptive tracking control for hypersonic vehicles with guaranteeing multi-performance requirements. *Aerosp. Sci. Technol.* **2020**, *105*, 106025. [CrossRef]

26. Ze, P.Z.; Fang, L.Z.; De, Z.X.; Zhi, F.G. An interval-estimation-based anti-disturbance sliding mode control strategy for rigid satellite with prescribed performance. *ISA Trans.* **2020**, *105*, 63–76. [CrossRef]

27. Xiu, W.H.; Guang, R.D. Fault-tolerant attitude tracking control of combined spacecraft with reaction wheels under prescribed performance. *ISA Trans.* **2020**, *98*, 161–172. [CrossRef]

28. Hirabayashi, M.; Kim, Y.; Brozović, M. Finite element modeling to characterize the stress evolution in Asteroid (99942) Apophis during the 2029 Earth encounter. *Icarus* **2021**, *365*, 114493.

29. Scheeres, D.J.; Wibben, D.; Antreasian, P.G.; Getzandanner, K.M.; Takahashi, S.; McMahon, J.W.; Lauretta, D. The Dynamics about Asteroid (101955) Bennu. In Proceedings of the AIAA SCITECH 2022 Forum, San Diego, CA, USA, 3–7 January 2022.

30. Terui, F.; Ogawa, N.; Ono, G. Guidance, navigation, and control of Hayabusa2 touchdown operations. *Astrodynamics* **2020**, *4*, 393–409.

31. Rusconi, M.; Ferrari, F.; Topputo, F. The effect of a rocky terrain for CubeSat landing on asteroid surfaces. *Adv. Space Res.* **2022**. [CrossRef]

32. Zeng, X.Y.; Wen, T.G.; Li, Z.; Alfriend, K.T. Natural Landing Simulations on Generated Local Rocky Terrains for Asteroid Cubic Lander. *IEEE Trans. Aerosp. Electron. Syst.* **2022**, *58*, 3492–3508.

33. Wen, T.G.; Zeng, X.Y.; Circi, C.; Gao, Y. Hop Reachable Domain on Irregularly Shaped Asteroids. *J. Guid. Control Dyn.* **2020**, *43*, 1269–1283. [CrossRef]

34. Zeng, X.Y. Li, Z.W.; Gan, Q.B.; Circi, C. Numerical Study on Low-Velocity Impact Between Asteroid Lander and Deformable Regolith. *J. Guid. Control Dyn.* **2022**, *45*, 1644–1660. [CrossRef]

35. Scheeres, D.; Gaskell, R.; Abe, S.; Barnouin-Jha, O.; Hashimoto, T.; Kawaguchi, J.; Kubota, T.; Saito, J.; Yoshikawa, M.; Hirata, N.; et al. The Actual Dynamical Environment About Itokawa. In Proceedings of the AIAA/AAS Astrodynamics Specialist Conference and Exhibit, Keystone, CO, USA, 21–24 August 2006. [CrossRef]

36. Niu, B.; Zhao, J. Barrier Lyapunov functions for the output tracking control of constrained nonlinear switched systems. *Syst. Control Lett.* **2013**, *62*, 963–971. [CrossRef]

37. Lian, B.; Bang, H. Momentum transfer-based attitude control of spacecraft with backstepping. *IEEE Trans. Aerosp. Electron. Syst.* **2006**, *42*, 453–463. [CrossRef]